

Report

**R-21-10**

September 2022



# iCP version 2.0 – A numerical tool for solving reactive transport in discrete fractures with matrix diffusion

**Diego Sampietro**

**María Pool**

**Elena Abarca**

**Jorge Molinero**

SVENSK KÄRNBRÄNSLEHANTERING AB

SWEDISH NUCLEAR FUEL  
AND WASTE MANAGEMENT CO

Box 3091, SE-169 03 Solna  
Phone +46 8 459 84 00  
skb.se

SVENSK KÄRNBRÄNSLEHANTERING



ISSN 1402-3091

**SKB R-21-10**

ID 1919443

September 2022

# **iCP version 2.0 – A numerical tool for solving reactive transport in discrete fractures with matrix diffusion**

Diego Sampietro, María Pool, Elena Abarca, Jorge Molinero  
Amphos 21 Consulting S.L.

This report concerns a study which was conducted for Svensk Kärnbränslehantering AB (SKB). The conclusions and viewpoints presented in the report are those of the authors. SKB may draw modified conclusions, based on additional literature sources and/or expert opinions.

This report is published on [www.skb.se](http://www.skb.se)

© 2022 Svensk Kärnbränslehantering AB



# Summary

A new version of iCP (interface COMSOL-PHREEQC) to solve reactive transport problems in fracture-matrix systems with matrix diffusion is presented.

In this approach, the fractures are modelled explicitly as discrete fractures, and, therefore, upscaling methods to convert a Discrete Fracture Network (DFN) to an Equivalent Continuous Porous Medium (ECPM) are not required. The rock matrix is modelled with 1D elements attached to the nodes of the discrete fractures. This additional geometrical dimension represents matrix diffusion processes and the reactivity of the matrix. With this 1D matrix approach, reactivity related to diffusion processes in the rock matrix can be simulated without a full three-dimensional representation of the matrix. The model treats the mineralogy and reactivity of the discrete fractures and the matrix individually. This approach allows to solve reactive transport problems in complex fracture-matrix systems considering networks composed of several thousand fractures.

Three benchmark problems of fracture-matrix systems are presented to validate the approach of representing the system with discrete fractures with 1D matrix as implemented in the new version of iCP. Both conservative and reactive transport problems are simulated. Additionally, other approaches such as Continuous Porous Media (CPM) and hybrid models have been considered for the sake of comparison. In CPM models both fractures, and the rock matrix are represented as a continuous porous medium. In hybrid models the fractures are discretized in one dimension less than the porous medium, and reactive transport problems can be solved in both the DFN and the matrix or only in the matrix with fractures acting as preferential paths for flow and transport.

The accuracy of the representation of a discrete fracture with 1D matrix as implemented in iCP has been evaluated through comparisons with results obtained from Pflotran, an open source, massively parallel flow and reactive transport code (Lichtner et al. 2015), from PHAST (Parkhurst et al. 2004) as well as from analytical solutions. Numerical results demonstrate that representing the rock matrix with 1D elements can correctly reproduce the effect of matrix diffusion processes and capture accurately the general geochemical behaviour of the systems evaluated. The slight discrepancy between the iCP model results and the results from the other models are caused by the different thermodynamic databases and kinetic models used.

Additionally, an application case, which considers a complex discrete fracture network of around 3 500 fractures with a 1D matrix representation is presented. The performance of this matrix-fractures representation is evaluated in terms of speed-up and computer resources demand. The performance analysis shows that the total simulation time with a 1D matrix is reasonable to solve complex and realistic problems.

This report is the second in a series of two reports that describe the development of iCP to handle reactive transport modelling in fractured media. The first report (Sampietro et al. 2022a) focuses on DFN and hybrid models, whereas this report focuses on DFN with an extra (spatial) dimension to model porous matrix transport.

# Sammanfattning

En ny version av iCP (gränssnitt COMSOL-PHREEQC) för reaktiv transportmodellering i sprickiga system presenteras. Med den nya versionen av iCP kan sprickor representeras av diskreta element och matrisen av 1D element. Denna 1D matris-metodik möjliggör beräkning av reaktiv transport i form av diffusion i matrisen utan att behöva representera matrisen i 3D. Metodiken tar hänsyn till den mineralogiska och reaktiva utvecklingen i sprickor och matris separat och möjliggör reaktiv transportmodellering i komplexa spricknätverk med fler tusen sprickor.

Tre typexempel på problemlösningar för konservativ och reaktiv transport i sprickiga system presenteras för att utvärdera den implementerade 1D matris-metodiken i iCP. Även ekvivalenta kontinuerliga porösa media (CPM) modeller och hybridmodeller har beaktats. I CPM-modeller representeras både sprickor och matris som ett kontinuerligt poröst medium. I hybridmodeller representeras sprickor av element som är av en lägre rumsdimension än det porösa mediet, och reaktiv transport kan lösas för både det diskreta spricknätverket och matrisen eller endast för matrisen med antagande om att sprickorna utgör preferentiella flödesvägar.

Den implementerade 1D matris-metodiken i iCP har utvärderats genom jämförelse med simuleringsresultat från Pflotran (Lichtner et al. 2015) och PHAST (Parkhurst et al. 2004) samt med analytiska lösningar. Numeriska simuleringsresultat visar att 1D matris-metodiken väl reproducerar effekten av matrisdiffusion och den generella geokemiska utvecklingen i system. Små skillnader mellan resultaten från iCP och de andra modellerna beror på implementering av olika termodynamiska databaser och kinetiska modeller.

Därutöver, har 1D matris-metodiken applicerats för ett spricknätverk med 3 500 sprickor. Prestandan för iCP med implementeringen av 1D matris-metodiken har utvärderats baserat på förkortad beräkningstid och åtgång av beräkningsresurser. Resultaten visar att den totala simuleringstiden vid implementering av denna metodik möjliggör analys av komplexa och realistiska sprickiga system.

Denna rapport är den andra av två rapporter som beskriver utvecklingen av iCP för reaktiv transportmodellering i sprickiga system. Den första rapporten (Sampietro et al. 2022a) fokuserar på diskreta spricknätverksmodeller (DFN-modeller) och hybridmodeller, medan denna rapport fokuserar på DFN-modeller där matrisen representeras av 1D element (1D matris-metodiken) som möjliggör beräkning av matrisdiffusion

# Contents

<b>1</b>	<b>Introduction</b>	7
1.1	Objective	9
<b>2</b>	<b>Numerical Approaches</b>	11
2.1	iCP to solve reactive transport in discrete fractures with 1D matrix	11
2.2	Pflotran	13
<b>3</b>	<b>Validation tests</b>	15
3.1	Benchmark 1: Conservative transport (Tang et al. 1981)	15
3.1.1	Description	15
3.1.2	Numerical implementation	16
3.1.3	Results	16
3.2	Benchmark 2: Infiltration of hyperalkaline groundwaters in calcitic dolomite along fractures	18
3.2.1	Description	18
3.2.2	Numerical implementation in iCP and Pflotran	20
3.2.3	Results	21
3.3	Benchmark 3: Matrix dissolution	24
3.3.1	Description	24
3.3.2	Numerical implementation in iCP and Pflotran	25
3.3.3	Results	26
<b>4</b>	<b>Application case to a three-dimensional DFN</b>	29
4.1	Description	29
4.2	Numerical implementation	29
4.3	Results	31
4.4	Performance quantification	34
<b>5</b>	<b>Conclusions</b>	37
	<b>References</b>	39



# 1 Introduction

Since 2013, consulting company Amphos 21 is working together with SKB in the context of the image platform (<https://image-modelling.net/>) to develop an interface that couples COMSOL Multiphysics (COMSOL 2017) and IPHREEQC (Charlton and Parkhurst 2011). This commercial interface is written in Java and uses the IPHREEQC C++ dynamic library and the COMSOL Java API. The resulting interface iCP (interface COMSOL-PHREEQC) (Nardi et al. 2014) is a powerful tool for solving a wide range of Multiphysics and chemical problems and it has been used by SKB to study the durability of the EBS systems in nuclear repositories (Idiart et al. 2019, 2020).

The first release of iCP was developed to solve THC (thermo-hydro-chemical) problems in porous media (Nardi et al. 2014). Recently, some additional developments have been carried out to increase the capabilities and efficiency of the software.

Since 2016, the focus has been on the development, testing and verification of a methodology for modelling flow and transport in discrete fracture networks in COMSOL Multiphysics and reactive transport in iCP. Numerical results (Sampietro et al. 2022b) have demonstrated the potential of the use of DFN to improve the understanding of the behaviour of groundwater flow in the backfill/rock interface of the BHA vault in the repository for long-lived waste (SFL). The implementation of DFN in COMSOL Multiphysics has been verified in terms of groundwater flow and conservative transport. Recent efforts related to the iCP\_DFN project have been focused on adapting iCP to solve reactive transport models (RTM) using DFN.

The traditional and probably the most used approach to simulate reactive transport problems in matrix-fracture systems is representing the fractured rock as a continuous porous medium (CPM) with upscaled and equivalent properties. However, this method usually requires very fine meshes to properly represent the fracture network. A different approach to solve reactive transport problems in fractured media consists of representing fractures as discrete structures (DFN). In this context, there are different models, which are summarized in Figure 1-1, depending on where and how the chemical reactions are solved:

- Pure DFN reactive transport models (RTM), which include chemical reactions only in the fractures. In this approach the thickness of the fracture is not explicitly modelled.
- Hybrid models in which fractures are embedded in a porous medium. The fractures are represented as discrete features using lower dimension finite elements than the porous medium, (e.g. 1D fractures crossing a 2D porous matrix or 2D fractures inside a 3D porous volume). Hybrid models can solve reactive transport in both the fractures and the matrix or assume reactions only in the matrix with fractures acting as preferential paths for flow and transport.
- Models of discrete fractures with 1D matrix, which also solve reactive transport both in fractures and in the matrix. However, in this approach the treatment of the matrix is simplified with respect to the hybrid approach. Thus, instead of a full 3D representation of the matrix, the matrix domain is represented as a set of independent 1D elements connected to the fractures. Thus, 2D transport processes in the matrix are neglected. This extra dimension approach can be applied only when the main mechanism for transport in the matrix is diffusion. For this approach, iCP uses the extra dimensions capabilities of COMSOL Multiphysics, which allow to simulate reactions and matrix diffusion processes by means of 1D elements that can be attached to complex geometries such as DFNs with thousands of fractures. The length of the extra dimension to represent the rock matrix depends on the specific problem to be solved, and it should be defined in terms of the average fracture half-spacing and the fracture aperture.

Figure 1-2 shows an example of an 1D fracture with the matrix represented as an extra dimension, where the rock matrix is represented as a set of 1D elements connected with the fracture. Transport in the 1D elements is governed by the Poisson partial differential equation. The fracture and the rock matrix are coupled by an exchange term. The developments carried out in the iCP code allow to include chemical reactions in both fracture and matrix.

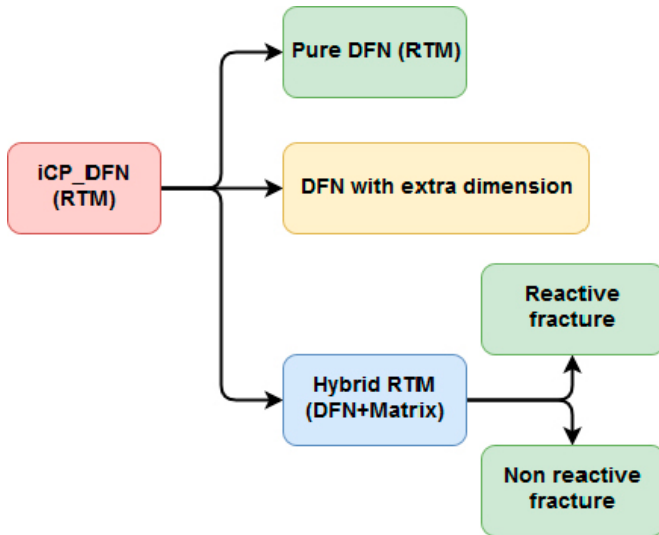


*Figure 1-1. Different approaches to deal with reactive transport models in discrete fracture networks.*

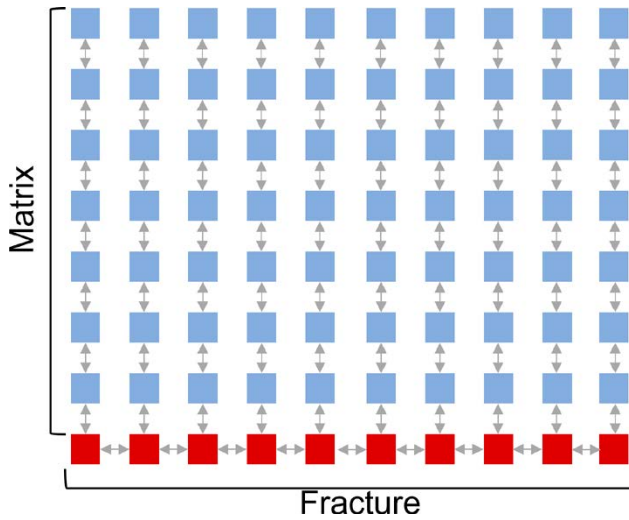


*Figure 1-2. Discretization of the fracture (red) and the matrix (blue). Note that both the fracture and the 1D elements of the extra dimension which represent the rock matrix can be discretized with several nodes.*

## 1.1 Objective

The main objective of this work is to present the capabilities of the new version of iCP (interface COMSOL-PHREEQC) to solve reactive transport in discrete fractures including diffusion and reactions into the rock matrix, which are simulated with a set of independent 1D elements connected to the fractures. With this approach reactivity related to diffusion processes in the rock matrix can be simulated without a full three-dimensional representation of the matrix. This approach can be applied only when diffusion is the main mechanism for transport in the matrix.

There is a lack of test cases available to validate these types of tools. For that reason, three validation tests involving a single fracture and matrix system are presented. In these tests, the results of iCP are compared against other codes and against other approaches in iCP (continuous porous medium and Hybrid RTM (Figure 1-1) with a full three-dimensional representation of the matrix).

The benchmarks are:

- First, a simple conservative transport problem in a single fracture-matrix system is presented to test the implementation of the non-reactive transport in fractures in iCP. In this case, numerical results are compared with results obtained from PHAST (Parkhurst et al. 2004), as well as with results from the analytical solution derived by Tang et al. (1981) and Sudicky and Frind (1982).
- Second, two more complex benchmark problems involving reactive transport in a single fracture have been performed to evaluate the performance of the new iCP version. Numerical results have been compared with results using Pflotran (Lichtner et al. 2015).
- Third, a 2D benchmark by Iraola et al. (2019) based on the calcite dissolution test of Pflotran (Lichtner et al. 2015).

This validation/benchmarking activity evaluates the iCP applicability to solve problems of fracture and matrix systems of interest in the near-field of radioactive waste repositories (e.g., SFR and SFL), such as the chemical degradation of fractured concrete or the improvement of the representation of the Excavation Damaged Zone (EDZ) and its impact on the release of radionuclides and concrete leaching water from the repository vaults to the geosphere.

The approach can be used in DFN, where fractures are explicitly resolved as discrete structures and, therefore, the upscaling of transport and geochemical properties to build an equivalent continuous porous medium is not required. The usability of this approach to solve reactive transport in complex geometries involving discrete fracture networks is illustrated with a 3D application of dolomitization in a fractured carbonate-rich rock containing 3 531 hexagonal fractures.



## 2 Numerical Approaches

Two different codes have been used to solve the benchmark problems presented: iCP, which couples COMSOL Multiphysics and PHREEQC (Nardi et al. 2014), and Pflotran (Lichtner et al. 2015). This chapter provides the governing equations of these two codes.

### 2.1 iCP to solve reactive transport in discrete fractures with 1D matrix

iCP (Nardi et al. 2014) is an efficient interface which couples two simulation programs: the general purpose finite element framework COMSOL Multiphysics (COMSOL 2017) and the geochemical simulator IPHREEQC (Charlton and Parkhurst 2011). iCP is written in Java and uses the IPhreeqc C++ dynamic library and the COMSOL Java API. It is distributed by Amphos 21 (<https://techlabs.amphos21.com/technology/interface-comsol-phreeqc/>). The current version 2.0 works with all COMSOL versions available in the market and uses the most updated IPhreeqc library. The main benefit of this interface is the possibility of coupling a wide range of Multiphysics problems with the powerful capabilities of IPHREEQC. COMSOL is used to simulate groundwater flow and transport of dissolved chemical species through porous and fractured media, as well as other physical processes such as heat transport or mechanical effects, and IPHREEQC is used to perform the geochemical calculations. Reactive transport is divided in two steps using an operator splitting technique with a sequential non-iterative approach.

A new version of iCP (interface COMSOL-PHREEQC) has been developed to solve reactive transport in discrete fractures including reactivity related to diffusion processes in the rock matrix. The extra-dimension capability in COMSOL is used to represent the processes in the matrix without the need of a full 3D representation of the matrix. This capability can be used to perform additional calculations over a geometry attached to the principal model geometry. Thus, models of different (or the same) dimensions can be connected. The additional dimensions are discretized with a finite element mesh over which partial differential equations (PDE) are solved. The connection between the two models can be defined mathematically by the user. In this particular case, the matrix is represented by 1D objects (lines) attached to a model of fractures, which are defined either as 1D or 2D objects (Figure 1-2). Thus, reactive transport is solved in both fractures and the rock matrix.

The groundwater flow in the fractured media is simulated using a combination of the Darcy's law (Darcy 1856) in a tangential form and the continuity equation, which is given by:

$$\vec{u}_f = -\frac{\vec{k}_f}{\mu} d_f (\vec{\nabla}_T p + \rho g \vec{\nabla}_T z) \quad (2-1)$$

where  $u_f$  [ $\text{m}^3_{\text{water}} \cdot \text{m}^{-1}_{\text{fracture}} \cdot \text{s}^{-1}$ ] is the volume flow rate per unit length in the fracture,  $k_f$  [ $\text{m}^2$ ] is the fracture permeability,  $d_f$  [ $\text{m}$ ] is the aperture of the fracture,  $\mu$  [ $\text{Pa} \cdot \text{s}$ ] is the viscosity,  $p$  [ $\text{Pa}$ ] is the pressure and  $g$  [ $\text{m} \cdot \text{s}^{-2}$ ] denotes the gravitational acceleration constant. The mean Darcian fluid velocity within fracture is defined as  $v_f = u_f/d_f$ .

A single governing equation for the fluid pressure can be obtained by combining Equation (2-1) with the continuity equation.

$$d_f \frac{\partial}{\partial t} (\phi_f \rho) + \vec{\nabla}_n \cdot (\rho \vec{u}_f) = d_f Q_f \quad (2-2)$$

where  $\phi_f$  [ $\text{m}^3_{\text{pores}} \cdot \text{m}^{-3}_{\text{medium}}$ ] is the fracture porosity and  $Q_f$  [ $\text{kg} \cdot \text{m}^{-3} \cdot \text{s}^{-1}$ ] is the mass source term.

It is important to notice that this equation solves only the fluid velocity within the fractures, and it does not consider the low permeable matrix.

For conservative transport in fractures with a 1D matrix, COMSOL solves two transport equations, one equation for fractures and another equation for the matrix. The transport equation for fractured media is written as:

$$d_f \left[ (\phi) \frac{\partial c_{i,f}}{\partial t} + \vec{\nabla}_T \cdot (\vec{I} D \vec{\nabla}_T c_i) + \vec{u} \cdot \vec{\nabla}_T c_i \right] = d_f R_i + n_o \quad (2-3)$$

where  $c_{i,f}$  [mol · kg<sub>w</sub><sup>-1</sup>] is the concentration of the chemical species  $i$  in the fracture,  $d_f$  [m] is the fracture thickness,  $I$  is the identity matrix,  $D$  [m<sup>2</sup> · s<sup>-1</sup>] is the effective diffusivity that includes the diffusion and dispersion processes and  $n_o$  [mol · m<sup>-2</sup> · s<sup>-1</sup>] corresponds to out-of-plane flux from the neighbouring porous domain.  $\vec{\nabla}_T$  denotes the gradient tangential to the fracture surface.

The transport equation for the matrix only considers the movement of the chemical species by diffusion. The resulting equation is similar to the Poisson equation and can be obtained by simplifying the Advection diffusion dispersion equation (Bear 1972), which yields

$$\phi_m \frac{\partial c_{i,m}}{\partial t} = \vec{\nabla} \cdot [\vec{I} D_e \cdot \vec{\nabla} c_i] + R_i \quad (2-4)$$

where  $c_{i,m}$  [mol · kg<sub>w</sub><sup>-1</sup>] is the concentration of the chemical species  $i$  in the matrix,  $\phi_m$  is the matrix porosity and  $D_e$  [m<sup>2</sup> · s<sup>-1</sup>] is the effective molecular diffusion of the chemical species.

At the contact between the rock matrix and the fracture, the coupling between the transport of aqueous species in the fractures and the transport of aqueous species in the porous medium ensures mass conservation. Hence, the solute mass flow per unit length of intersection entering the fracture,  $j_f^{int}$  [mol · m<sup>-1</sup> · s<sup>-1</sup>], equals the solute mass flow per unit length of intersection leaving the porous medium,  $j_m^{int}$ , or viceversa.

$$j_f^{int} + j_m^{int} = 0 \quad (2-5)$$

The fracture-matrix coupling is performed using a Cauchy-type boundary condition where the mass flow between fractures and rock matrix is proportional to the difference in concentration in the fracture ( $c_f$ ) and in the matrix ( $c_m$ ). This coupling is given by

$$\begin{cases} j_f^{int} = -\beta(c_m - c_f) \\ j_m^{int} = \beta(c_m - c_f) \end{cases} \quad (2-6)$$

where  $\beta$  [m<sup>2</sup> · s<sup>-1</sup>] is the mass transfer coefficient.

Figure 2-1 shows the behaviour of the boundary condition as a function of  $\beta$ . The Cauchy boundary condition can cover the range between a prescribed pressure boundary condition ( $\beta = \infty$ ) and a no-flow boundary condition ( $\beta = 0$ ). For values of  $\beta$  larger than a threshold  $\beta_p$ , the boundary condition behaves as a prescribed pressure (Dirichlet) boundary condition and the flow through the interface is independent of the value of  $\beta$ . For values of  $\beta$  lower than  $\beta_p$ , the boundary condition behaves as a prescribed flow (Neumann) boundary condition. The value of the mass flux ( $J$ ) in those cases depends on the value of  $\beta$ . As a result, there is a concentration discontinuity between the discrete fractures and the porous medium at the interface. The value of  $\beta_p$  is problem dependent and should be estimated with a set of conservative preliminary simulations.

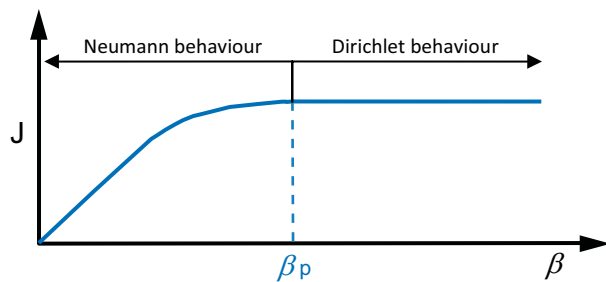


**Figure 2-1.** Behaviour of the Cauchy boundary condition as a function of the conductance,  $\beta$ . For values larger than  $\beta_p$ , the mass flux remains constant and the concentration in the fracture and in the matrix is equal in the shared nodes.

Assuming that there is a physical interface or layer between the porous medium and the fracture that is not explicitly modelled, the physical meaning of the coefficient of proportionality  $\beta$  can be extracted from Fick's law integrated over the fracture aperture  $d_f$  (m). Thus,  $\beta = d_f D_{int}/b_{int}$ , where  $D_{int}$  is the diffusivity at the interface between the porous medium and the fracture, and  $b_{int}$ , the thickness of the layer. This type of boundary condition allows to represent several physical processes such as barrier resistance or sealing of the fracture. It acts as a continuity condition when  $\beta$  tends to infinity and as a zero flux when  $\beta$  tends to zero.

On the other hand, the reactive transport problem is performed with IPHREEQC which solves a set of algebraic differential equations. The reactive system consists of a set of ordinary differential equations representing kinetic reactions

$$\begin{cases} \frac{du_g}{dt} + \frac{du_m}{dt} + \frac{du_a}{dt} + \frac{du_d}{dt} = r_{kin} \\ f(u, c, r_{kin}, T) = 0 \end{cases} \quad (2-7)$$

where  $u = Uc$  [ $\text{mol} \cdot \text{kg}_w^{-1}$ ] is the vector of components with  $U$  the component matrix, and  $T$  [ $^{\circ}\text{C}$ ] is the temperature. The subscripts refer to the subcomponent in phase gas ( $g$ ), mineral ( $m$ ), aqueous ( $a$ ) and sorbed ( $d$ ), respectively. Thus, the conservative concentrations of the dissolved species computed in Equations (2-4) and (2-5) are included as  $u_a$  in the IPHREEQC step, Equation (2-7).

The chemical system solved in IPHREEQC consists of a set of ordinary differential equations (ODE) associated to kinetic reactions, and a set of algebraic equations which arise from the formulation of components  $u$ , the mass action law, the water activity model used to represent non-ideal solutions, etc. Furthermore, IPHREEQC also includes the usually non-linear expressions that relate  $u$ ,  $c$ , and  $r_{kin}$  and also  $T$  (for non-isothermal problems). The complete formulation can be found in the PHREEQC user guide (Parkhurst and Appelo 2013).

## 2.2 Pflotran

PFLOTRAN (Lichtner et al. 2015) is an open source, state-of-the-art, massively parallel flow and reactive transport code which solves a system of generally nonlinear partial differential equations describing multiphase, multicomponent and multiscale reactive flow and transport in porous materials.

PFLOTRAN's Richard mode is used to solve fluid mass conservation. This mode is based on the Richard's equation for a single phase, variably saturated, incompressible isothermal flow. The governing mass conservation equation is given by

$$\frac{\partial}{\partial t}(\varphi s \eta) + \nabla \cdot (\eta \mathbf{q}) = Q_w \quad (2-8)$$

with the Darcy flux,  $\mathbf{q}$ , defined as

$$\mathbf{q} = \frac{k k_r(s)}{\mu} (\nabla P - \rho \mathbf{g}) \quad (2-9)$$

Here,  $\varphi$  [-] is the porosity,  $s$  [-] is the saturation,  $\eta$  [ $\text{kmol} \cdot \text{m}^{-3}$ ] is the molar water density,  $\rho$  [ $\text{kg} \cdot \text{m}^{-3}$ ] denotes water density,  $\mathbf{q}$  [ $\text{m} \cdot \text{s}^{-1}$ ] is the Darcy flux,  $k$  [ $\text{m}^2$ ] the intrinsic permeability,  $k_r$  [-] is the relative permeability,  $\mu$  [ $\text{Pa} \cdot \text{s}$ ] is the viscosity,  $P$  [ $\text{Pa}$ ] is the pressure and  $\mathbf{g}$  [ $\text{m} \cdot \text{s}^{-2}$ ] denotes the gravitational acceleration constant. The considered source/sink term  $Q_w$  [ $\text{kmol} \cdot \text{m}^{-3} \cdot \text{s}^{-1}$ ] can be written as:

$$Q_w = \frac{q_M}{W_w} \delta(\mathbf{r} - \mathbf{r}_{ss}) \quad (2-10)$$

where  $q_M$  [ $\text{kg} \cdot \text{m}^{-3} \cdot \text{s}^{-1}$ ] denotes a mass rate,  $W_w$  [ $\text{kg} \cdot \text{kmol}^{-1}$ ] is the molar mass of water,  $\mathbf{r}_{ss}$  denotes the location of the source/sink and  $\delta(x)$  is the Dirac delta function.

Various relative permeability functions ( $k_r(s)$ ) are supported, including Van Genuchten, Brooks-Corey and Thomeer-Corey. However, in this work all the simulations are considered to be fully saturated, and then the relative permeability functions are not used.

The governing mass conservation equations for reactive transport describe geochemical transport for a multiphase system written in terms of a set of independent aqueous primary species, and read as:

$$\frac{\partial}{\partial t}(\varphi \sum_{\alpha} s_{\alpha} \Psi_j^{\alpha}) + \nabla \cdot \sum_{\alpha} \Omega_j^{\alpha} = Q_j - \sum_m v_{jm} I_m - \frac{\partial S}{\partial t} \quad (2-11)$$

$$\frac{\partial \varphi_m}{\partial t} = \bar{V}_m I_m \quad (2-12)$$

The rate of change of the  $m$ -th mineral volume fraction  $\varphi_m$  [ $\text{m}^3_{\text{mineral}} \cdot \text{m}^3_{\text{medium}}$ ] is expressed as a function of the molar volume  $\bar{V}_m$  [ $\text{m}^3 \cdot \text{mol}^{-1}$ ] and mineral reaction rate  $I_m$  [ $\text{mol} \cdot \text{s}^{-1}$ ]. The subscript  $\alpha$  refers to the fluid phase,  $v_{jm}$  [-] represents the reaction stoichiometry, and the quantity  $\Psi_j^{\alpha}$  [ $\text{mol} \cdot \text{m}^{-3}$ ] denotes the total concentration of the  $j$ -th primary species ( $A_j^{pri}$ ) in the  $\alpha$ -th fluid phase. The total flux  $\Omega_j^{\alpha}$  for species-independent diffusion is given by:

$$\Omega_j^{\alpha} = (q_{\alpha} - \varphi s_{\alpha} D_{\alpha} \cdot \nabla) \Psi_j^{\alpha} \quad (2-13)$$

where  $\varphi$  [-] is the porosity and  $D_{\alpha}$  [ $\text{m}^2 \cdot \text{s}^{-1}$ ] is the diffusion/dispersion tensor which may be different for different phases. The diffusivity/dispersivity tensor  $D_{\alpha}$  is the sum of contributions from molecular diffusion and dispersion, and is given by

$$D_{\alpha} = \tau D_m \mathbf{I} + \alpha_T \nu \mathbf{I} + (\alpha_L - \alpha_T) \frac{\nu \nu}{\nu} \quad (2-14)$$

where  $\alpha_L$  and  $\alpha_T$  [m] are the longitudinal and transverse dispersivities, respectively, and  $\tau$  is the tortuosity and  $D_m$  [ $\text{m}^2 \cdot \text{s}^{-1}$ ] is the molecular diffusion coefficient.

The quantity  $Q_j$  in Equation 2-11 denotes a source/sink term defined as:

$$Q_j = \sum_n \frac{q_M}{\rho} \Psi_j \delta(r - r_n) \quad (2-15)$$

where  $q_M$  [ $\text{kg} \cdot \text{m}^{-3}$ ] denotes a mass rate,  $\rho$  [ $\text{kg} \cdot \text{m}^{-3}$ ] denotes the fluid density,  $r_n$  refers to the location of the  $n$ -th source/sink and  $\delta(x)$  is the Dirac delta function.

### 3 Validation tests

Three benchmark problems are performed for the verification of iCP to solve reactive transport in discrete fractures with 1D matrix. Benchmark 1 simulates conservative transport in a single fracture-matrix system including matrix diffusion. Benchmark 2 is based on the example presented by Steefel and Lichtner (1998), which describes multicomponent reactive transport in a planar fracture-matrix system. Benchmark 3 is based on a test of Pflotran (Lichtner et al. 2015) presented by Iraola et al. (2019), which solves calcite dissolution processes in a planar fracture-matrix system.

The details of the validation tests and the comparison between results from the literature and numerical results by using iCP and Pflotran are outlined in the following subsections.

#### 3.1 Benchmark 1: Conservative transport (Tang et al. 1981)

##### 3.1.1 Description

The first benchmark reproduces conservative transport in a single fracture-matrix system including matrix diffusion. In this case, the analytical solution by Tang et al. (1981) is used to test the implementation of the non-reactive transport in fractures in COMSOL Multiphysics.

The model domain consists of a single fracture-matrix system where the fracture presents a uniform aperture and parallel walls. Due to the fact that the domain is symmetric along the fracture, only half the real fracture aperture is explicitly included in the model (see Figure 3-1).

Solute transport in the fracture is dominated by advection from left to right, whereas diffusion is the only mechanism for transport in the matrix. A fixed concentration boundary condition is applied at the inlet of the fracture, and a constant outflow is imposed at the outlet. The rest of the boundaries present no flow boundary conditions. Parameters used for the simulations are summarized in Table 3-1.

**Table 3-1. Parameters used for the benchmark 1.**

Parameter	Value	Description
$\sigma$ (m)	0.1	Fracture aperture half-width
$L$ (m)	100	Fracture length
$b$ (m)	1.0	Matrix Domain
$\varphi_f$ (-)	0.5	Fracture porosity
$\varphi_m$ (-)	0.001	Matrix porosity
$D_g$ (m <sup>2</sup> /s)	$1.0 \times 10^{-14}$	Effective Diffusion coefficient
$v$ (m/s)	$1.59 \times 10^{-7}$	Velocity in the fracture
$C$ (mg/L)	1.0	Tracer concentration

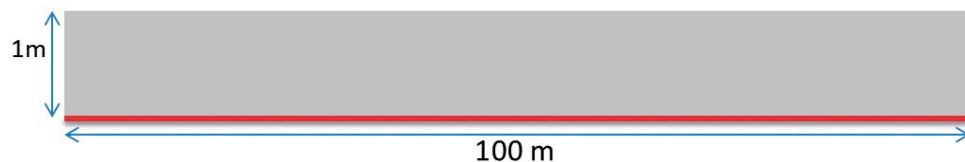


**Figure 3-1.** Schematic representation of the conceptual model. The red line represents half of the fracture, and the grey region represents the rock matrix.

### 3.1.2 Numerical implementation

Benchmark 1 represents a conservative transport problem and, therefore, it can be solved directly in COMSOL without using iCP. However, iCP has been used for this benchmark to validate the coupling between COMSOL and IPHREEQC.

For simplicity, the fracture is oriented along the x-axis and the matrix along the z-axis, which points vertically upward (see Figure 3-2). The model setup can be conceptualized using different matrix and fracture dimensions:

- A. 3D continuous porous media (3D CPM). Both the matrix and the fracture are considered 3D entities with one element in the y-direction. Thus, the fracture is modelled as a continuous 3D porous medium.
- B. Hybrid 3D-2D (hybrid 3D2D). The matrix is considered to be a 3D domain with one element in the y-direction, and the fracture is defined as a 2D discrete fracture. Therefore, this configuration consists of a hybrid method with 3D porous materials and 2D discrete features.
- C. 2D continuous porous media (2D CPM). The matrix and the fracture are represented by two different 2D domains. This configuration uses a continuous porous media approach.
- D. Hybrid 2D-1D (hybrid 2D1D). In this case, the model uses a hybrid method with a 2D matrix and a 1D fracture.
- E. Discrete fractures with 1D matrix. The fracture is represented by one 1D discrete element and the rock matrix is represented by 1D elements.

Although representing the rock matrix with 1D elements requires a lower complexity of the finite element mesh, the number of elements is similar to that for the case with a 2D explicit matrix (D in Figure 3-2). It is important to mention that the interchange between the 1D matrix elements is not simulated, that is 2D diffusion processes into the matrix are neglected.

### 3.1.3 Results

The validation of the model is carried out by comparing the breakthrough curves (normalized concentration vs. time) at the fracture outlet obtained from iCP, Pflotran and PHAST (Parkhurst et al. 2004) with the analytical solution presented by Tang et al. (1981).

Figure 3-3 shows numerical and analytical results of the breakthrough curves obtained after 10000 years of simulations. Note that for the first 750 years, all numerical results are in good agreement with the analytical solution. However, after this time, all numerical results show a significant increase in the tracer concentration with respect to one predicted by the analytical solution. This overestimation in the concentration is due to boundary effects. That is, after 750 years the tracer in all models reaches the boundary and the assumption of a semi-infinite domain is no longer valid.

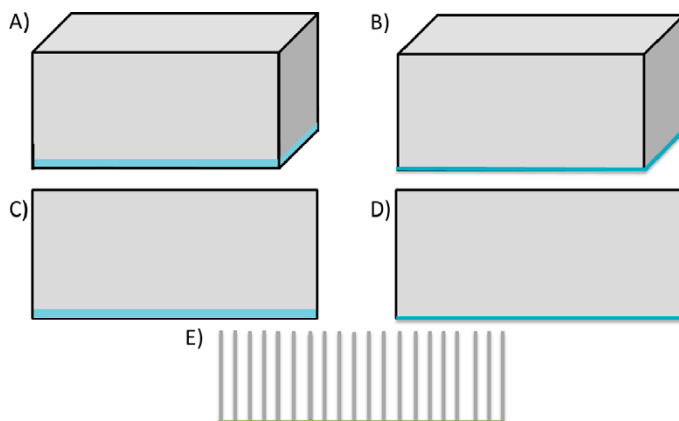


**Figure 3-2.** Different conceptualizations of the matrix and fracture, A) 3D continuous porous media including the matrix and the fracture, B) hybrid model with a 3D domain representing the rock matrix and a 2D discrete fracture, C) 2D continuous porous media including the matrix and the fracture, D) hybrid model with a 2D domain representing the rock matrix and a 1D discrete fracture and E) 1D discrete fracture with 1D matrix.

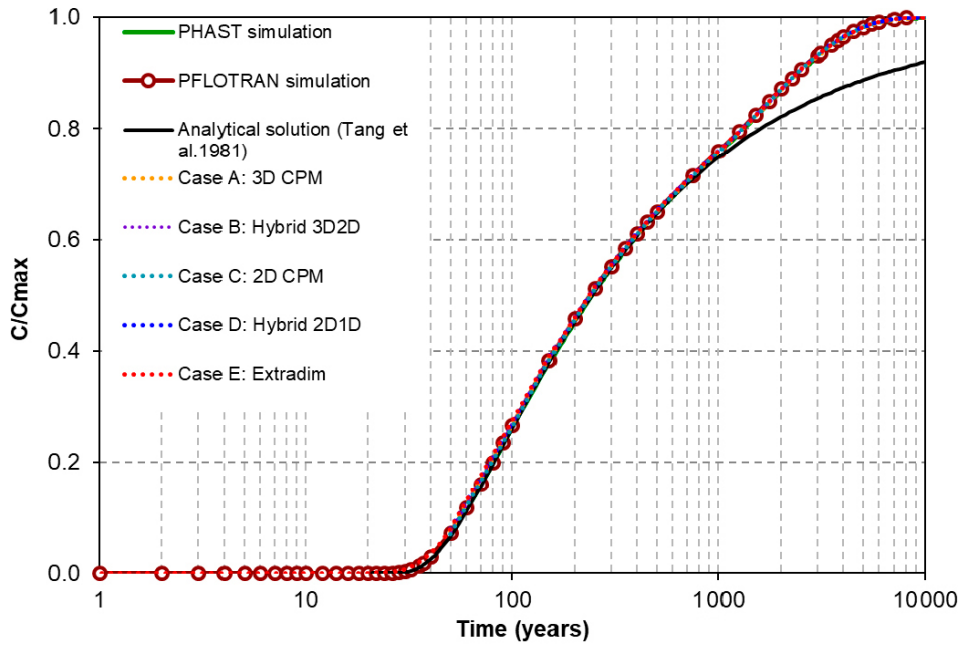


**Figure 3-3.** Breakthrough curves of normalized tracer concentration ( $C/C_{max}$ ) at the fracture outlet ( $x=100$  m). The black solid line represents the analytical solution, the red circles Pflotran numerical results, the green solid lines the PHAST simulations and the dotted lines results from COMSOL for the different conceptualizations considered.

Note also that results for simulation Case E (discrete fracture with 1D matrix, red dotted line in Figure 3-3) are identical to ones obtained for the other model configurations (Case A-D).

Table 3-2 shows the number of elements, degrees of freedom and computational times used in COMSOL Multiphysics for the different model configurations. All the simulations have been performed using a linear discretization of the finite elements. Note that the fastest simulation corresponds to the case with a 2D discrete fracture and a 2D matrix. The high computation time for the discrete fracture with 1D matrix case is due to the complexity of the equations solved for this system.

For cases A-D, the numerical method used imposes continuity between the matrix and the fracture. That is, the concentration along the fracture is imposed to be the same as the one at the nodes which connect the fracture and the matrix. This assumption simplifies the solved system and increases the speed-up of the models. However, this assumption implies that the fracture and the matrix have the same chemical behaviour, which might not be a realistic assumption in several geochemical systems. This limitation motivates the development of the coupling approach (defined in Equation (2-5) and (2-6)) to represent the connection between the fracture and rock matrix through the mass transfer coefficient  $\beta$ . Thus, small values of  $\beta$  are adequate to represent a weak connection between the fracture and the matrix, whereas large values should be considered when chemical continuity exists (see Section 2.1 for more details). This approach allows to define different concentrations of the chemical species in the fracture and the adjacent matrix allowing to handle both with different geochemical composition. This coupling methodology is used for the hybrid (Figure 1-1) and the discrete fractures with 1D matrix configurations.

On the other hand, the discrete fracture with 1D matrix increases the complexity of the system of PDEs solved and, therefore, the computational time increases (from 20 seconds for the 2D1D configuration to 31 seconds for the discrete fracture with 1D matrix). These results are obtained using a similar discretization of the matrix for all the cases analysed. However, the computation time of model E can be reduced to 10 seconds just by reducing the number of the 1D elements which represent the matrix.

**Table 3-2. Computer speed-up and degrees of freedom for the different model configurations in COMSOL Multiphysics. The simulations were run on a computer with a i7-8700 processor with a CPU speed of 3.7 GHz, 6 cores and 64 GB of RAM memory.**

Model	N° of elements	Number of degrees of freedom	Computational time (s)
A	31 700	23 517	199
B	29 744	22 311	24
C	20 400	20 703	20
D	20 000	20 301	23
E	100 for the fracture and 15 for each extra dimension	18 895	31

## 3.2 Benchmark 2: Infiltration of hyperalkaline groundwaters in calcitic dolomite along fractures

### 3.2.1 Description

Benchmark 2 investigates the physical and chemical controls on an alteration front geometry in a discrete fracture system including precipitation and dissolution processes. This example was presented by Steefel and Lichtner (1998).

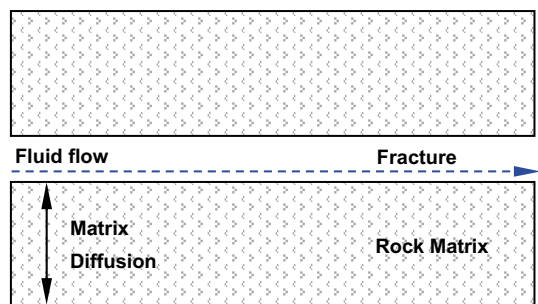
This test considers a thin non-deformable single fracture developed within a 2D saturated porous rock matrix. The fracture has a constant aperture half-width of 0.645 mm, and planar parallel walls. A constant flow velocity is imposed at the inlet of the fracture, and flow within the rock matrix is considered to be negligible, Figure 3-4.

A typical Na–HCO<sub>3</sub> groundwater composition in equilibrium with the calcite and dolomite is considered as initial condition in the fracture and the matrix. A groundwater equilibrated with portlandite, brucite, and calcite is imposed at the inlet of the fracture. Groundwater composition for the initial and the boundary conditions used are the same as the ones defined by Steefel and Lichtner (1998), see Table 3-3.

**Table 3-3. Initial and boundary conditions used in benchmark 2.**

Component	Initial concentration (mol/L)	Concentration at the fracture inlet (mol/L)
Total Na <sup>+</sup>	$5.0 \times 10^{-2}$	$5.0 \times 10^{-2}$
Total Ca <sup>2+</sup>	$9.7 \times 10^{-4}$	$1.7 \times 10^{-2}$
Total Mg <sup>2+</sup>	$6.1 \times 10^{-5}$	$2.5 \times 10^{-8}$
Total CO <sub>2</sub>	$2.0 \times 10^{-3}$	$1.6 \times 10^{-6}$
Total Cl <sup>-</sup>	$5.0 \times 10^{-2}$	$5.0 \times 10^{-3}$
I(M)	$5.3 \times 10^{-2}$	$9.7 \times 10^{-2}$
Alkalinity	$2.0 \times 10^{-3}$	$3.49 \times 10^{-2}$
T (°C)	25	25
pH	8.00	12.39
log P <sub>CO<sub>2</sub></sub>	-3.0	-12.90

Equilibrium constants for mineral and aqueous complexation reactions used in the calculation are shown in Table 3-4. Mineral rate constants and surface areas considered are shown in Table 3-5.



No flow boundary

Figure 3-4. Conceptual model for benchmark 2 (modified from Steefel and Lichtner 1998).

Table 3-4. Reactions and equilibrium constants considered in benchmark 2.

Reaction	Log $K_{eq}$
$\text{OH}^- + \text{H}^+ \rightleftharpoons \text{H}_2\text{O}$	14.00
$\text{HCO}_3^- \rightleftharpoons \text{CO}_3^{2-} + \text{H}^+$	-10.33
$\text{CO}_2(\text{aq}) \rightleftharpoons \text{CO}_3^{2-} + 2\text{H}^+$	-16.67
$\text{NaHCO}_3(\text{aq}) \rightleftharpoons \text{CO}_3^{2-} + \text{H}^+ + \text{Na}^+$	-10.48
$\text{NaCO}_3^- \rightleftharpoons \text{CO}_3^{2-} + \text{Na}^+$	-0.51
$\text{NaOH}(\text{aq}) + \text{H}^+ \rightleftharpoons \text{Na} + \text{H}_2\text{O}$	14.80
$\text{MgCO}_3(\text{aq}) \rightleftharpoons \text{CO}_3^{2-} + \text{Mg}^{2+}$	-2.98
$\text{MgHCO}_3^+ \rightleftharpoons \text{CO}_3^{2-} + \text{H}^+ + \text{Mg}^{2+}$	-11.37
$\text{MgOH}^+ + \text{H}^+ \rightleftharpoons \text{Mg}^{2+} + \text{H}_2\text{O}$	11.97
$\text{MgCl} + \text{H}^+ \rightleftharpoons \text{Mg}^{2+} + \text{Cl}^-$	0.13
$\text{CaHCO}_3^+ \rightleftharpoons \text{CO}_3^{2-} + \text{H}^+ + \text{Ca}^{2+}$	-11.38
$\text{CaOH}^+ + \text{H}^+ \rightleftharpoons \text{Ca}^{2+} + \text{H}_2\text{O}$	12.85
$\text{Calcite} \rightleftharpoons \text{Ca}^{2+} + \text{CO}_3^{2-}$	-8.48
$\text{Dolomite} \rightleftharpoons \text{Ca}^{2+} + \text{Mg}^{2+} + \text{CO}_3^{2-}$	-18.14
$\text{Brucite} + 2\text{H}^+ \rightleftharpoons \text{Mg}^{2+} + 2\text{H}_2\text{O}$	16.30
$\text{Portlandite} + 2\text{H}^+ \rightleftharpoons \text{Ca}^{2+} + 2\text{H}_2\text{O}$	22.56

Table 3-5. Reaction rate constants and surface areas used in the calculations in benchmark 2.

Mineral	Log $K_s$ (moles/m <sup>2</sup> /s)	Surface area (m <sup>2</sup> <sub>mineral</sub> / m <sup>3</sup> <sub>medium</sub> )
Calcite	-6.19	500
Dolomite	-7.70	500
Brucite	-8.00	500

Proportions of 20, 50 and 30 % of the rock are considered for calcite, dolomite and porosity, respectively. Other parameters used for the simulations are summarized in Table 3-6.

Table 3-6. Parameters used for the simulations in benchmark 2.

Parameter	Value	Description
$L$ (m)	40	Fracture length
$\sigma$ (m)	$0.946 \times 10^{-3}$	Fracture aperture half-width
$\varphi_f$ (-)	1	Fracture porosity
$\varphi_m$ (-)	0.3	Matrix porosity
$D_e$ (m <sup>2</sup> /s)	$5.1 \times 10^{-10}$	Effective Diffusion coefficient
$v$ (m/s)	$3.17 \times 10^{-5}$	Velocity in the fracture

### 3.2.2 Numerical implementation in iCP and Pflotran

Steeffel and Lichtner (1998) used a modified version of the code GIMRT (Steeffel and Yabusaki 1996) which uses a global implicit or one-step method to couple transport and reaction. For the spatial discretization, a constant grid spacing of 1 m along the fracture and 0.5 mm perpendicular to the fracture was considered.

The benchmark has been reproduced by using two different codes: Pflotran and iCP. For the Pflotran application, the system has been conceptualized by including the fracture and matrix explicitly as an equivalent porous medium (CPM). For the iCP application, three different model configurations have been defined. First, a model setup which includes the fracture-matrix system explicitly as an equivalent porous medium (2D2D), Figure 3-5 left. Second, a model setup which considers explicitly the porous matrix and the fracture is represented as a discrete feature of 1 dimension (1D2D), Figure 3-5 right. Third, a model setup which includes the fracture as a 1D discrete feature, and the matrix is represented with 1D elements (1D-extradim).

For flow boundary conditions, all the cases in iCP consider a constant flow velocity along the fracture, and an outflow boundary condition at the outlet. A fixed concentration boundary condition is imposed at the inlet of the fracture. The chemical composition of the boundary water is shown in Table 3-3. The rest of the boundaries are considered no-flow boundaries. The initial composition of the water is detailed in Table 3-3.

The reactive transport model has been solved using a modified version of the CEMDATA database (Jacques 2009). The main difference between the geochemical model in iCP presented here and the one described in Steeffel and Lichtner (1998) is the mineral kinetic precipitation/dissolution rates. Steeffel and Lichtner (1998) used a generic kinetic rate solved implicitly in the reactive transport equation, whereas iCP uses IPHREEQC to solve the geochemical reactions, where the kinetic rates are written by the user. For this particular application, the following kinetic rate,  $r_{min}$ , is defined in iCP:

$$r_{min} = S_{surf} \cdot \phi \cdot K_s \cdot (1 - 10^{Si_{min}}) \quad (3-1)$$

where, the subscript min refers to the mineral phases considered (calcite, dolomite and brucite),  $S_{surf}$  [ $\text{m}^2 \cdot \text{m}^{-3}$ ] is the specific surface,  $K_s$  [ $\text{moles} \cdot \text{m}^{-2} \cdot \text{s}^{-1}$ ] is the kinetic rate (given in Table 3-5) and  $Si_{min}$  [-] refers to the saturation index of the mineral phase.

For the 1D2D and 1D-extradim models the mass transfer coefficient,  $\beta$  coefficient in Equation (2-6), is required to couple the rock matrix with the fracture. Because continuity in the concentration between the matrix and the fracture was imposed in the example presented by Steeffel and Lichtner (1998), a value of  $1 \cdot 10^{-4}$  [ $\text{m}^2 \cdot \text{s}^{-1}$ ] is assumed for  $\beta$ . This value is larger than the threshold  $\beta_p$  for this problem, and therefore the boundary condition behaves as a prescribed concentration (Dirichlet) boundary condition (see Section 2.1 for more details).

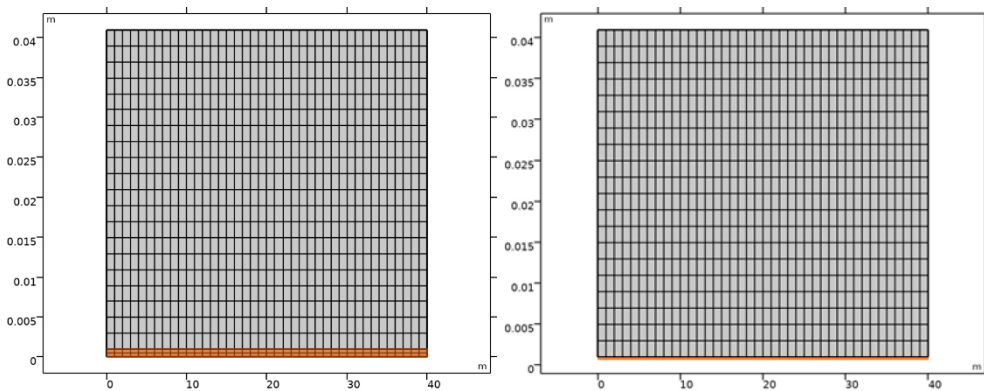


**Figure 3-5.** iCP finite element mesh for benchmark 2. The grid for the 2D2D iCP model consists of 880 elements (left) and for the 1D2D iCP model 800 elements are used (right). The orange surface and line show the location of the fracture. Note that the vertical axis is exaggerated 1000 times compared to the horizontal.

In iCP, the time step is one of the critical parameters to ensure accuracy and numerical stability. Thus, the time step should be small enough to satisfy both the Courant and von Neumann criteria (Parkhurst and Appelo 2013).

The Courant criterion relates the time-step size with the spatial discretization and the fluid velocity,  $v$  (m/s), and reads as:

$$\frac{v\Delta t}{\Delta x} \leq 1 \quad (3-2)$$

Based on the Courant criterion, the time step defined in the iCP simulations is 31 600 seconds.

On the other hand, for the Pflotran application, a 3D domain including explicitly both the fracture and the matrix is considered. For the initial flow condition, a hydrostatic pressure is considered in both the rock matrix and the fracture to simulate fully saturated conditions. A prescribed flux is imposed at the inlet of the fracture with a Dirichlet zero gradient boundary condition for transport. This implies a prescribed concentration on inflow and zero diffusive gradient on outflow (i.e., only advective transport is considered on outflow). At the outlet of the fracture a prescribed flux with a zero-gradient boundary (zero diffusive gradient for outflow) is imposed. The rest of the boundaries are set to no flow of both solute and water, that is, flow within the rock matrix is considered negligible. The resident and boundary water considered are specified in Table 3-3.

### 3.2.3 Results

Dolomitization processes with a calcite precipitation peak are expected to occur only in diffusion-dominated systems (Steefel and Lichtner 1994). In this problem, although transport in the fracture is mainly dominated by advection, the coupling of diffusion and reaction in the rock matrix induces diffusion-controlled reactive processes in the fracture. Thus, a reaction front with a calcite precipitation peak results in the fracture due to the interplay between mixing and matrix diffusion.

Figure 3 in Steefel and Lichtner (1998) illustrates the calcite precipitation rate,  $\text{Ca}^{2+}$ ,  $\text{CO}_3^{2-}$  and solution pH after 50 years of simulations. A calcite precipitation peak occurs in both the fracture and the matrix. On the other hand, the pH decreases from the inlet of the fracture and evolves to a constant value at a distance from where the calcite precipitation rate is zero. The pH, ion concentration and mineral reaction rate profiles in the fracture show the same behaviour as the ones in the rock matrix where transport is purely diffusion-dominated.

In the matrix, numerical results presented by Steefel and Lichtner (1998) demonstrated that the reaction front is controlled by the Peclet number, which does not depend on mineral reaction kinetics and is defined as  $P_e = \sigma v / \phi_m D_a$ , where  $v$  is the fracture velocity,  $\sigma$  is the fracture aperture half-width,  $\phi_m$  is the matrix porosity, and  $D_a$  is the effective diffusion coefficient.

Numerical results also demonstrated that the Peclet number can be used as a scaling factor to predict solute concentration, reaction rate, and volume fraction profiles along the fracture from the scaling of the reaction front in the matrix. Thus, Figure 4 in Steefel and Lichtner (1998) provides evidence that solution pH and calcite precipitation rate in the matrix scaled by the Peclet number reproduces the shape observed along the fracture.

Numerical results using Pflotran for solution pH, calcite precipitation rate and calcium concentration are shown in Figure 3-6. These results are very similar to the ones presented by Steefel and Lichtner (1998) for the spatial distribution of pH and major ions.

Figure 3-7 illustrates solution pH and calcite precipitation rate along the fracture and in the matrix scaled by the Peclet number. Numerical results using Pflotran slightly overestimate the calcite precipitation peak and underestimate the calcite precipitation rate before the peak with respect to the results presented by Steefel and Lichtner (1998). On the other hand, the Pflotran simulation reproduces properly the fit between the profile along the fracture and the scaled front in the matrix.

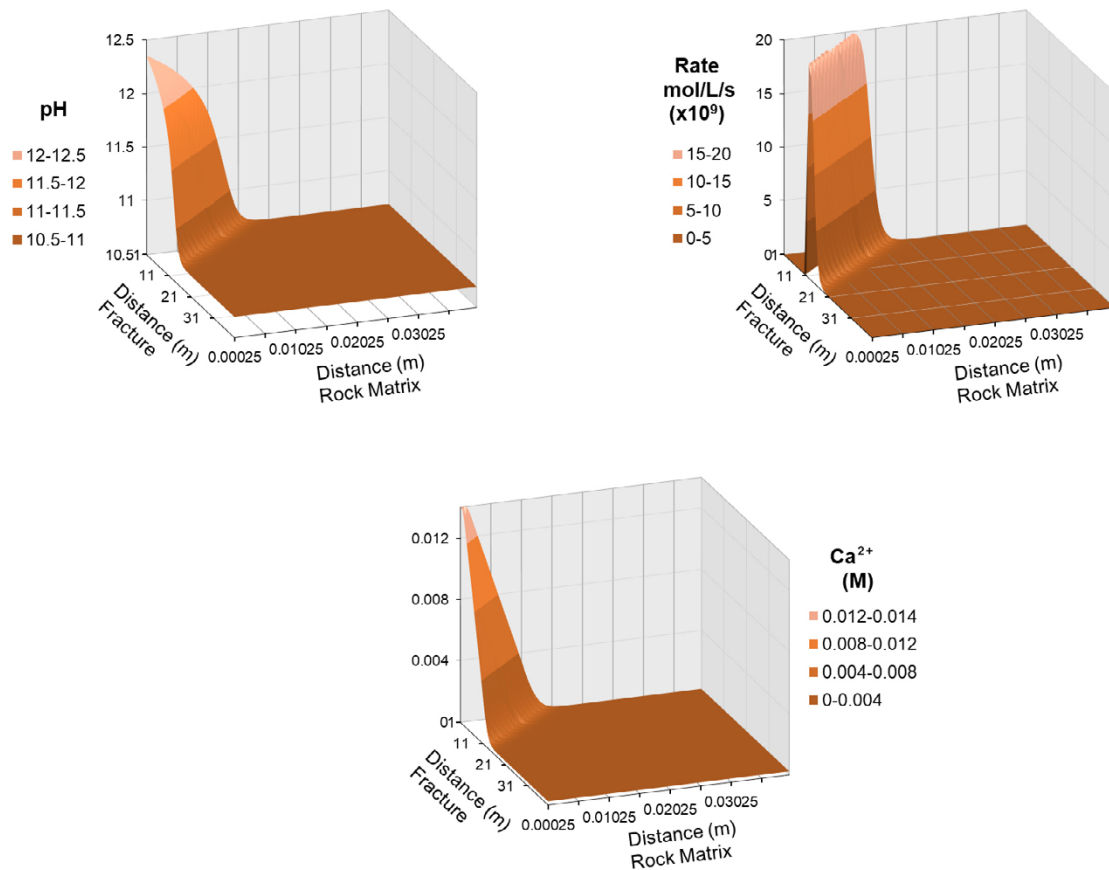


**Figure 3-6.** Pflotran results for solution pH, calcite precipitation rate, and  $\text{Ca}^{2+}$  concentrations after 50 years of simulation.

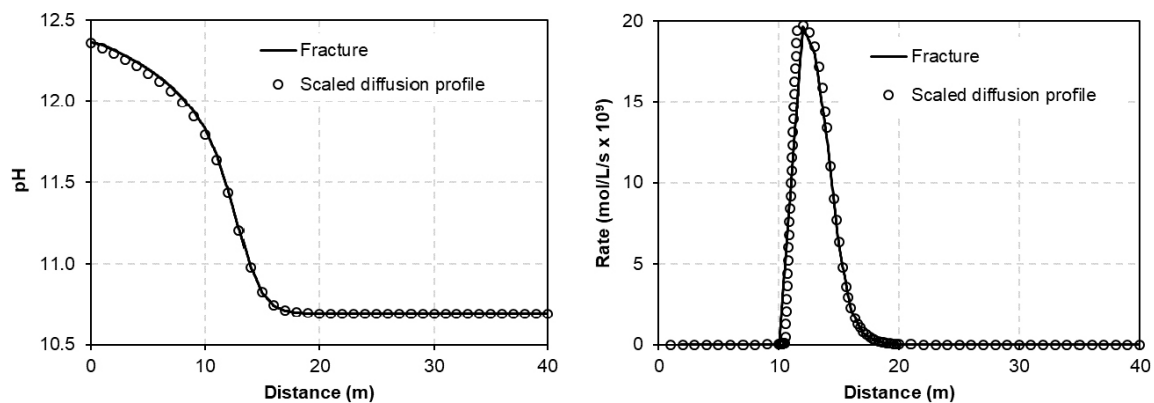


**Figure 3-7.** Pflotran results for solution pH and calcite precipitation rate in the fracture and in the matrix scaled by the Peclet number after 50 years of simulations.

Numerical results for solution pH, calcium and carbon concentration from iCP with the 2D2D model setup are shown in Figure 3-8. Note that iCP results are in good agreement with numerical results presented by Steefel and Lichtner (1998) and also with numerical results from Pflotran (Figure 3-6). Thus, iCP results correctly reproduce the diffusion-controlled reactive processes in the fracture.

On the other hand, differences in the thermodynamic equilibrium constant of the minerals used in the iCP database and by Steefel and Lichtner (1998) lead to a slightly different pH of equilibrium. Thus, iCP results predict a minimum pH of 11, whereas Steefel and Lichtner (1998) reported a pH of 10.8. The differences in the chemical formulations (chemical database and kinetic rates) might also explain the discrepancies in the concentrations of the dissolved species between the codes used.

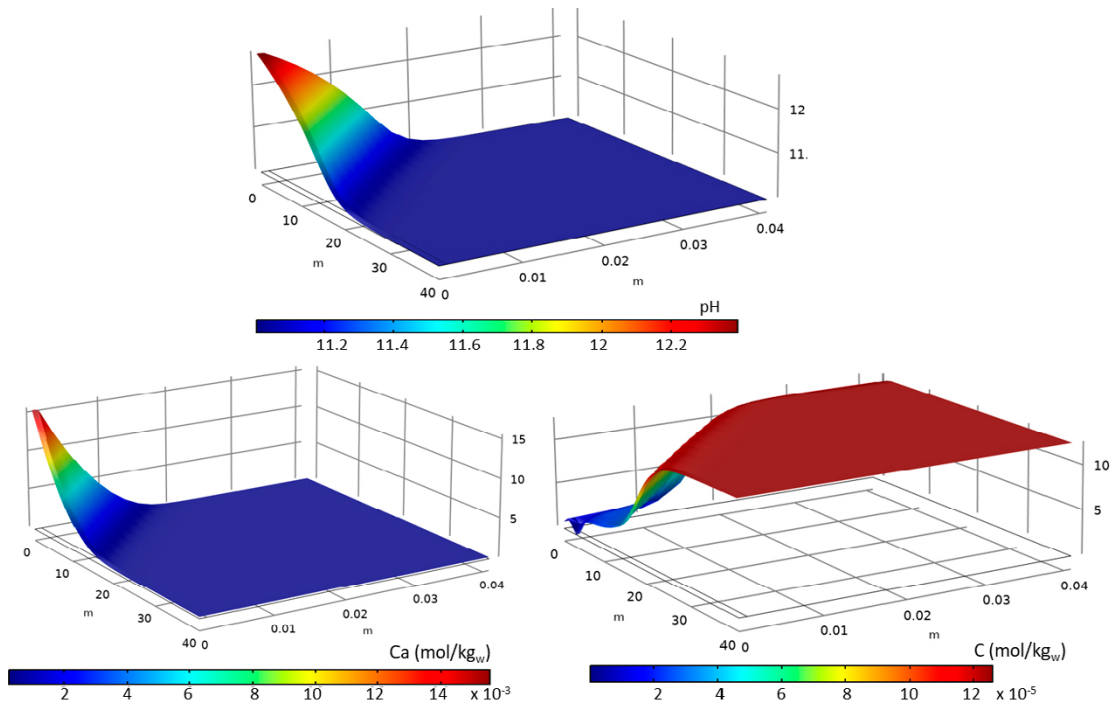


**Figure 3-8.** iCP results for solution pH, total dissolved calcium and carbon concentrations after 50 years of simulation using the 2D2D model.

Figure 3-9 illustrates iCP results of solution pH and calcite precipitation rate along the fracture and the matrix scaled by the Peclet number for the three setups considered. Note that iCP numerical results (scaled by the Peclet number) properly reproduce the chemical composition along the fracture and the matrix. However, the precipitation rate obtained from iCP is different to the one presented by Steefel and Lichtner (1998) and also to the one obtained from Pflotran. Thus, iCP results show a constant rate from the inlet of the fracture which decreases gradually after 10 m without the existence of the calcite precipitation peak. These differences are due to the thermodynamic database used. Particularly, Steefel and Lichtner (1998) stated that the boundary water defined for this problem (see chemical composition in Table 3-3) was in equilibrium with calcite and dolomite. However, the resulting boundary water is slightly oversaturated with respect to calcite and dolomite when using the CEMDATA database and the same chemical composition. This oversaturation might explain the larger precipitation rate observed close to the fracture inlet.

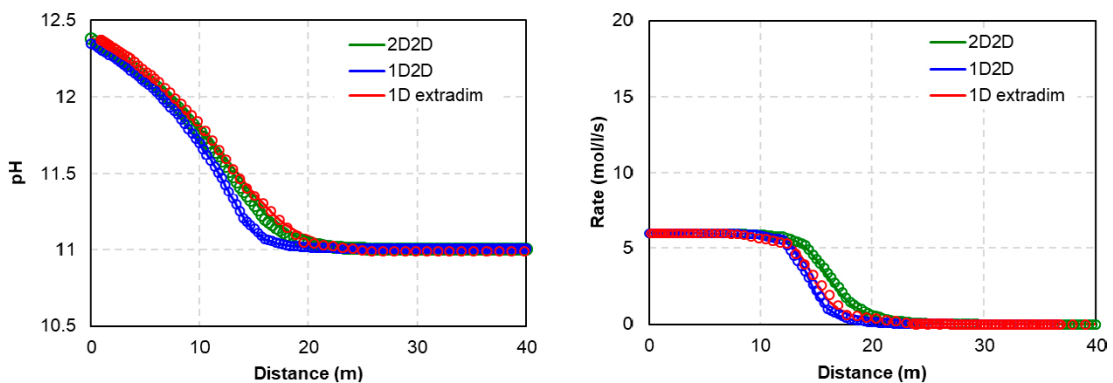


**Figure 3-9.** iCP results for solution pH (left) and calcite precipitation rate (right) in the fracture (continuous line) and in the matrix scaled by the Peclet number (circles) after 50 years of simulation for the three different models analysed.

It is also important to mention that very similar results are obtained when considering the different iCP model configurations. Thus, results for the 1D-extradim configuration are in good agreement with results obtained with the 2D2D and 1D2D setups. This comparison demonstrates that the model of discrete fracture with 1D matrix is appropriate to reproduce complex chemical dynamics in fracture-matrix systems.

### 3.3 Benchmark 3: Matrix dissolution

#### 3.3.1 Description

This benchmark is based on the calcite dissolution test of Pflotran (Lichtner et al. 2015) presented by Iraola et al. (2019). The conceptual model consists of the same geometrical setup with a single planar fracture-matrix system as the ones defined in benchmark 1 and 2, see Figure 3-4.

The rock matrix is formed mainly by calcite with a porosity of 1 %. Initially, the system is equilibrated with the resident water, which is in equilibrium with calcite (basic pH). The fracture has a constant aperture and planar parallel walls. At the inlet of the fracture an acidic water is injected at a constant rate, which leads to the dissolution of calcite. Parameters used in the simulations are listed in Table 3-7.

**Table 3-7. Parameters used for the simulations in benchmark 3.**

Parameter	Value	Description
$L$ (m)	0.5	Fracture length
$\sigma$ (m)	$1.58 \times 10^{-3}$	Fracture aperture half-width
$\varphi_r$ (-)	1	Fracture porosity
$\varphi_m$ (-)	0.01	Matrix porosity
$D_a$ (m <sup>2</sup> /s)	$1.0 \times 10^{-10}$	Effective Diffusion coefficient
$v$ (m/s)	$7.6 \times 10^{-7}$	Velocity in the fracture

The system is described by only three primary species, see Table 3-8 and Table 3-9. That is, secondary species are not included in the model. The evolution of the system is monitored by computing breakthrough curves at the fracture outlet.

**Table 3-8. Initial and boundary conditions used in benchmark 3.**

Component	Initial concentration (mol/L)	Concentration at the fracture inlet (mol/L)
Total Ca <sup>2+</sup>	$1.0 \times 10^{-6}$	$5.2 \times 10^{-4}$
Total HCO <sub>3</sub> <sup>-</sup>	$1.0 \times 10^{-3}$	$1.7 \times 10^{-3}$
T (°C)	25	25
pH	5.0	8.0

Equilibrium constants and mineral rate constants and surface areas considered are shown in Table 3-9 and Table 3-10, respectively.

**Table 3-9. Reactions and equilibrium constants considered in benchmark 3.**

Reaction	Log $K_{eq}$
CaCO <sub>3</sub> (Calcite) + H <sup>+</sup> $\rightleftharpoons$ Ca <sup>2+</sup> + HCO <sub>3</sub> <sup>-</sup>	1.85

**Table 3-10. Reaction rate constants and surface areas used in benchmark 3.**

Mineral	Log $K_s$ (moles/m <sup>2</sup> /s)	Surface area (m <sup>2</sup> <sub>mineral</sub> / m <sup>3</sup> <sub>medium</sub> )
Calcite	-6.00	1

### 3.3.2 Numerical implementation in iCP and Pflotran

For the iCP application, two different model configurations are considered. The first model setup includes explicitly the matrix, and the fracture is represented by a 2D line. The second model represents a discrete fracture with 1D matrix. The same discretization with 250 elements in the direction along the fracture and 50 elements in the direction perpendicular to the fracture are used in both model setups. The size of the matrix element is finer in the area close to the fracture where the highest concentration gradients are expected (Figure 3-10).

Similar boundary conditions are considered in both model configurations (see Table 3-8). The concentration of ions in the boundary water is prescribed at the inlet of the fracture using a fixed concentration boundary condition. An outflow boundary condition is imposed at the outlet of the fracture. No advection nor diffusion is considered at the rest of the boundaries. It is important to mention that in this benchmark only the transport problem is solved in the iCP model. Thus, instead of solving the flow problem by prescribing the velocity at the inlet of the fracture as for the Pflotran model, in the iCP model the flow velocity along the fracture is prescribed as a constant value in the advection-dispersion equation, Equation (2-3).

For reactive transport, a modified version of the PHREEQC database (PHREEQC.dat) (Parkhurst and Appelo 2013) is considered. As for benchmark 2, the main difference between the geochemical model in iCP and the one presented by the authors is the kinetic precipitation/dissolution mineral rate used. iCP uses the same kinetic rate as the one used in benchmark 2, Equation (3-1) with parameters given in Table 3-10, which are different than the ones detailed in Iraola et al. (2019). The time step is small enough (85 seconds) to ensure numerical stability.

A 2D model, including the fracture explicitly, is also set up in Pflotran. For the spatial discretization, a constant refinement is considered with 250 grid cells in the direction parallel to the fracture and 750 cells in the perpendicular direction, with a total of 187 500 grid cells. A steady-state, uniform velocity is imposed along the fracture. A Dirichlet zero-gradient boundary condition for transport is imposed at both the inlet and outlet of the fracture.

The Pflotran input files for this benchmark are made available in a public GitLab repository, [https://github.com/aitorig/Benchmarking\\_dual\\_continuum\\_method\\_for\\_multicomponent\\_reactive\\_transpor-Supplementary\\_material](https://github.com/aitorig/Benchmarking_dual_continuum_method_for_multicomponent_reactive_transpor-Supplementary_material), (Iraola et al. 2019).

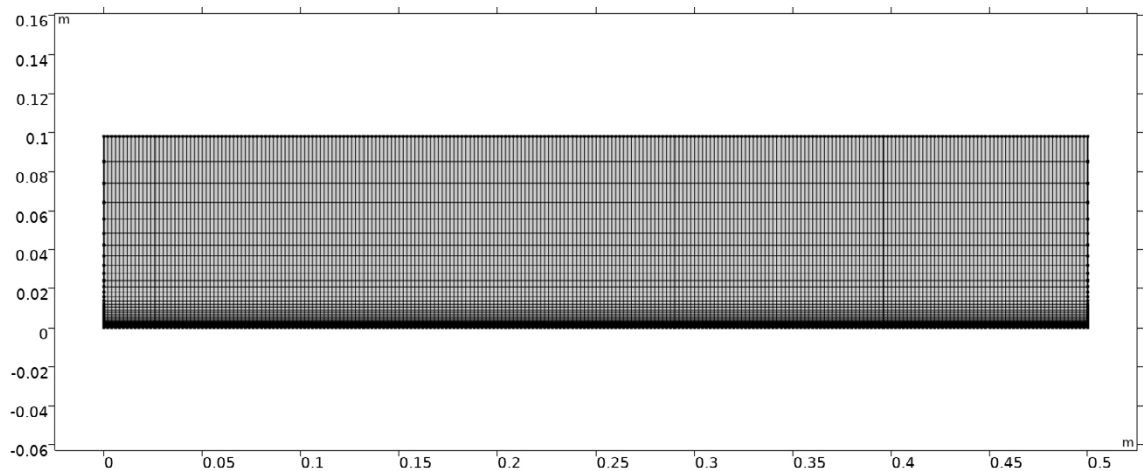


**Figure 3-10.** iCP finite element mesh for benchmark 3. The grid consists of 12 500 quadrilateral elements that represent explicitly the rock matrix.

### 3.3.3 Results

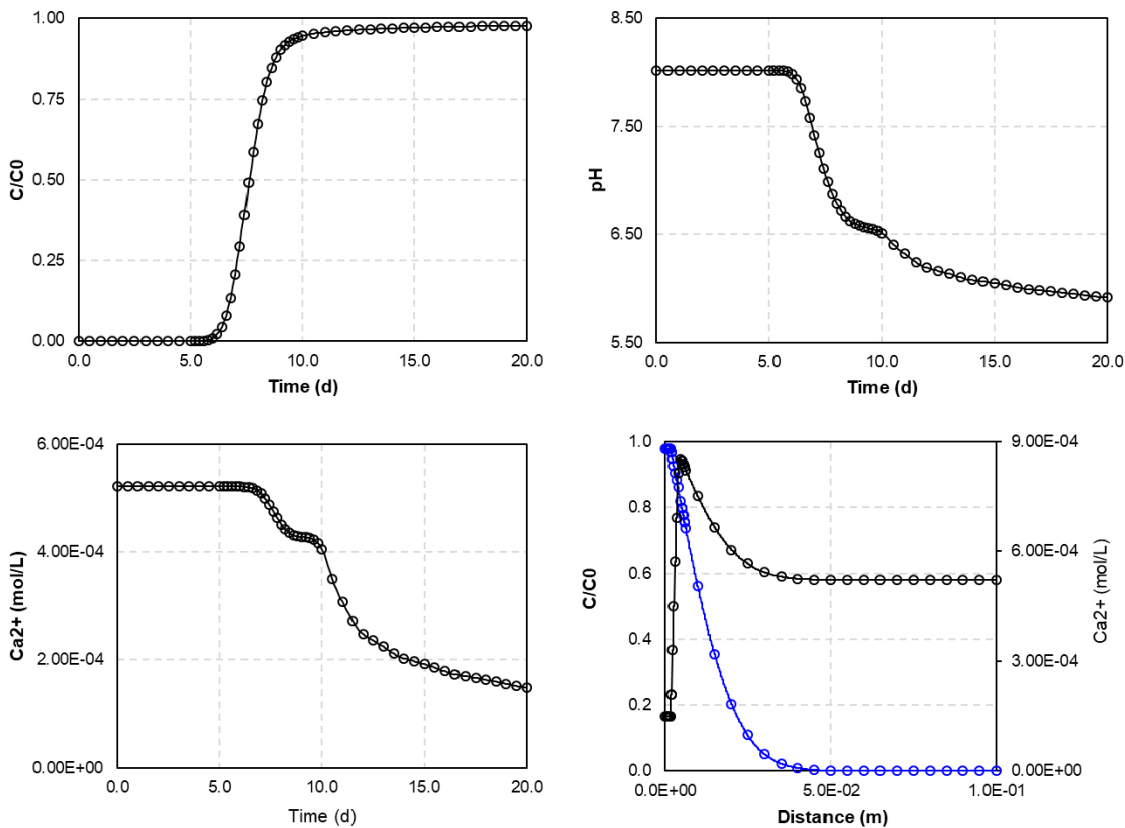
Pflotran numerical results for the breakthrough curve, temporal evolution for pH and  $\text{Ca}^{2+}$  concentration at the outlet of the fracture and profiles of tracer and  $\text{Ca}^{2+}$  concentration in the matrix taken in a transect perpendicular to the fracture at the fracture outlet are shown in Figure 3-11. Tracer concentration is normalized by the concentration prescribed at the fracture inlet.

Figure 3-12 illustrates Pflotran and iCP numerical results for the breakthrough curve of a non-reactive tracer and results obtained from the analytical solution (Tang et al. 1981). Note that both iCP and Pflotran accurately reproduce the analytical solution.

Pflotran and iCP results in terms of temporal evolution of pH and  $\text{Ca}^{2+}$  concentration at the fracture inlet are displayed in Figure 3-13 and Figure 3-14, respectively. Note that the iCP results for the two setups considered show a slower decrease in pH and  $\text{Ca}^{2+}$  concentration than the one observed with Pflotran. Thus, although the pH decreases after 5 days for all cases simulated, the pH obtained by the iCP models at the end of the simulation is lower than the one obtained with Pflotran. That is, the iCP model predicts a lower buffer capacity of the matrix.

Similar trends are obtained for the calcium ion concentration (Figure 3-14). Thus, iCP models predict a sharper decrease in the calcium concentration with time than the Pflotran model. Note also that the Pflotran model predicts a stepped breakthrough curve which is not reproduced by the iCP models. One probable explanation for the difference in the results is the different thermodynamic equilibrium constant and kinetic models employed.

It is important to note that results from iCP with the two setups considered are almost identical (Figure 3-13 and Figure 3-14). This agreement demonstrates the accuracy of the system as a discrete fracture with 1D matrix.



**Figure 3-11.** Pflotran results for the breakthrough curves of the conservative tracer; temporal evolution of pH and  $\text{Ca}^{2+}$  concentration at the outlet of the fracture, and profiles of tracer and  $\text{Ca}^{2+}$  concentration in the matrix in a transect perpendicular to the fracture and located at the fracture outlet after 20 days of simulations.

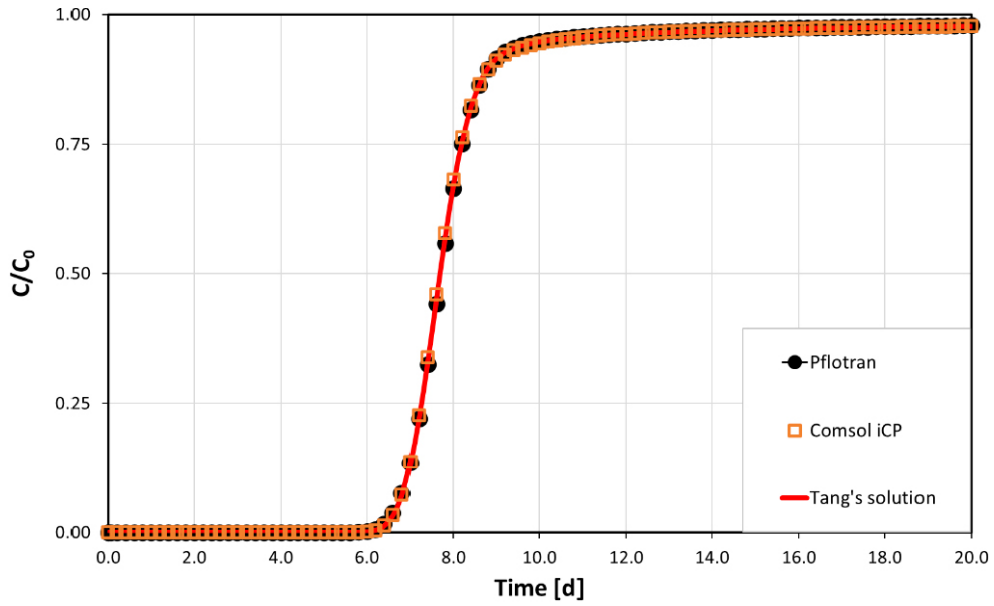


**Figure 3-12.** Breakthrough curves of the conservative tracer obtained when representing a discrete fracture with 1D matrix with COMSOL/iCP, including the matrix explicitly with Pflotran and from Tang's analytical solution.

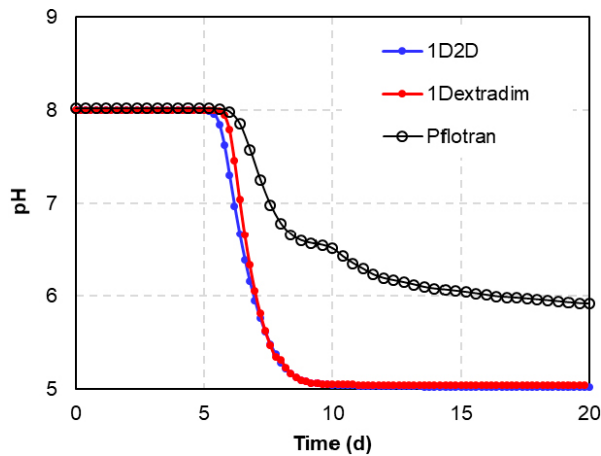


**Figure 3-13.** Comparison of Pflotran and iCP results for the pH evolution at the outlet of the fracture.

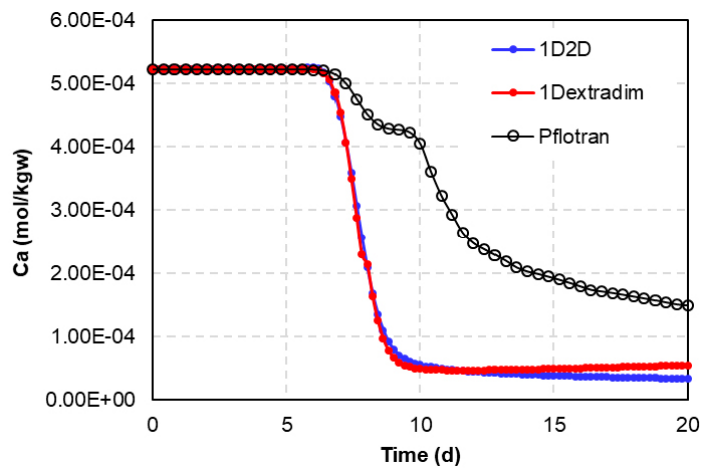


**Figure 3-14.** Comparison of Pflotran and iCP results for the temporal evolution of calcium concentration at the outlet of the fracture.



## 4 Application case to a three-dimensional DFN

In order to evaluate the performance of representing the rock matrix with 1D elements with iCP a more complex geometry with a 3D discrete fracture network is considered. Here, the performance is evaluated in terms of speed-up and computer resources demand. The presented 3D element mesh is also used to analyse the computational efficiency of this approach for more realistic and complex geometries. To this end, CPU times for the different steps of the reactive transport problem are quantified.

### 4.1 Description

A 3D fractured rock with carbonate minerals exposed to a constant circulation of groundwater that contains magnesium chloride is considered. In this system, magnesium-rich groundwater flows through the fractures leading to calcite dissolution and eventually dolomite formation. The fracture system is based on a discrete fracture network (DFN) generated in FracMan (Ford et al. 2008), which consists of 3 531 hexagonal fractures inside a cube of 200 m of length centered at origin (Figure 4-1). The hydraulic properties of the fractures (hydraulic conductivity, aperture and storativity) are spatially heterogeneous.

The chemical composition of the initial and boundary waters is given in Table 4-1. The matrix initially contains  $2 \times 10^{-4}$  moles/kg<sub>medium</sub> of calcite. In this system, transport is dominated by advection through the fractures. The travel time through the materials is long enough to assume local chemical equilibria and hence the dissolution/precipitation of calcite and dolomite is considered to occur in equilibrium.

**Table 4-1. Initial and boundary conditions used in the calculations.**

Component	Initial concentration (mol/kg <sub>w</sub> )	Concentration at the fracture inlet (mol/kg <sub>w</sub> )
Ca	$1.227 \times 10^{-4}$	$1 \times 10^{-14}$
C	$1.227 \times 10^{-4}$	$1.7 \times 10^{-14}$
Mg	$1.0 \times 10^{-5}$	$1.0 \times 10^{-3}$
Cl	$1.0 \times 10^{-4}$	$2.0 \times 10^{-3}$
T (°C)	25	25
Pe	4	4
pH	7.0	7.0

### 4.2 Numerical implementation

The geometry and properties of the discrete fracture network (Figure 4-1) generated in FracMan (Ford et al. 2008) are included in a .fab file. This is a standard file generated by the programs specialized in the generation of stochastic discrete fracture network such as DarcyTools (Svensson et al. 2010), Connectflow (Jacobs 2021) or FracMan (Ford et al. 2008). This .fab file contains information of the coordinates of the fractures as well as their hydraulic and transport properties (transmissivity, aperture and storativity). The geometry contained in the file is imported into COMSOL using a COMSOL utility app that generates the planar fractures and assigns the properties (transmissivity and aperture). The COMSOL application spends around half an hour reading the .fab file and building the fracture network.

The geometry extracted from the .fab file is formed by a set of fractures with a preferential orientation along the *x*-axis which is detailed in Figure 4-1. Note that two sets of fractures with different orientations can be identified: a set of fractures with a predominant horizontal dip; and another set of fractures with vertical dip along the *z*-axis. The size of the fractures is spatially variable. The fractures are represented as ideal 2D planes, and the aperture of each fracture is used in the transport equation

(Equation (2-2)). Due to the complexity of the fracture network, in this example the matrix is not modelled explicitly, but it is represented with 1D elements. For the sake of simplicity, the average fracture spacing was not considered to define the length of the extra dimension and a constant length of 1 m was set to represent the rock matrix with one finite element (two nodes). Thus, each node of the fracture is connected with a linear element according to the scheme in Figure 1-2. Therefore, the total number of nodes for the reactive transport simulation is three times the number of nodes for the groundwater flow simulation (Figure 4-1).

For boundary conditions, prescribed hydraulic heads (Dirichlet boundary condition) are imposed at the intersection of the fractures with the  $y$ - $z$  planes to generate a head gradient along the  $x$ -axis, with  $h = 1$  m for  $x = -100$  m and  $h = 0$  m for  $x = 100$  m, see Figure 4-2 and Figure 4-3. The rest of the boundaries are set to no-flow in terms of both solute and water flow. Initially, the groundwater flow is solved to reach the steady state solution. The reactive transport simulation covers a total simulation time of 210 years. The  $\beta$  coefficient of Equation (2-6) is set to  $1 \times 10^{-7} \text{ m}^2 \cdot \text{s}^{-1}$ , a value close to zero to consider possible concentration discontinuities between the matrix and the fractures. The chemical composition of the fracture-matrix system and the incoming water is summarized in Table 4-1. Figure 4-2 shows a schematic representation of the boundary conditions and transmissivity values considered.

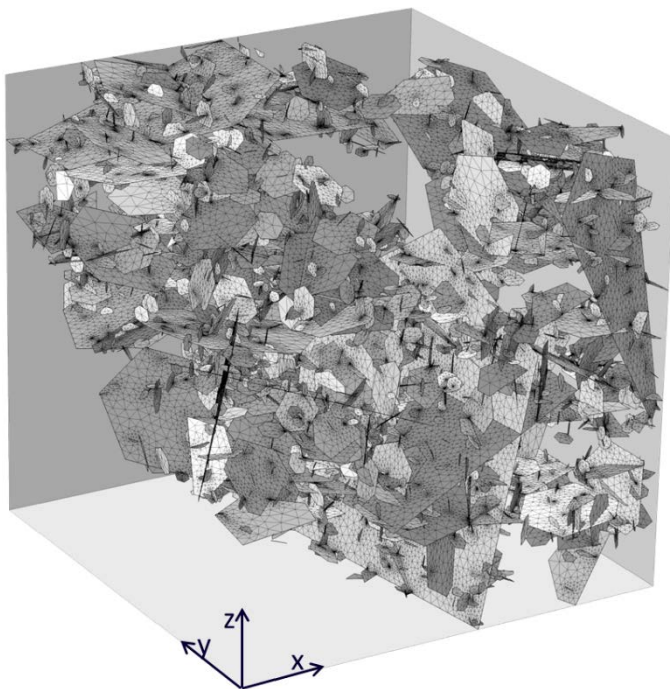


**Figure 4-1.** Mesh used for the application test. The grid is formed by 240 721 triangular elements which supposes a total of 130 979 nodes.

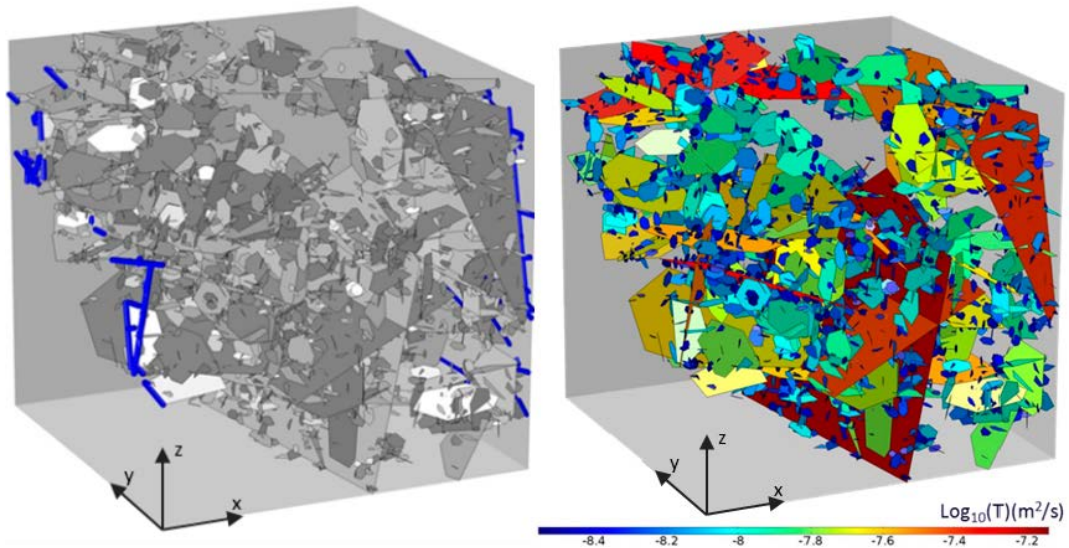


**Figure 4-2.** Left: Schematic description of the flow boundary conditions showing the edges with a Dirichlet boundary condition (blue lines). Right: Transmissivity values for the fractures in logarithmic scale for the DFN case.

### 4.3 Results

Numerical results from the flow simulation show a groundwater gradient along the  $x$ -axis and two preferential flow paths: one at the top of the model domain and the other one at the middle part (Figure 4-3). These paths are mainly controlled by the largest and most connected structures. The rest of the fractures present lower flow velocities because they are not well-connected or are even disconnected with the two main set of fractures. Note also that, in general, the low transmissivity values considered in the fractures induce low flow velocities (Figure 4-4).

For the flow balance, the total amount of water entering the system is  $3.44 \times 10^{-6}$  kg/s with a relative mass balance error of 2.2 %. This balance represents only the fractures. The finite element mesh is formed by 240 721 elements and the CPU time required to reach steady state flow conditions is 3 minutes (Table 4-2).

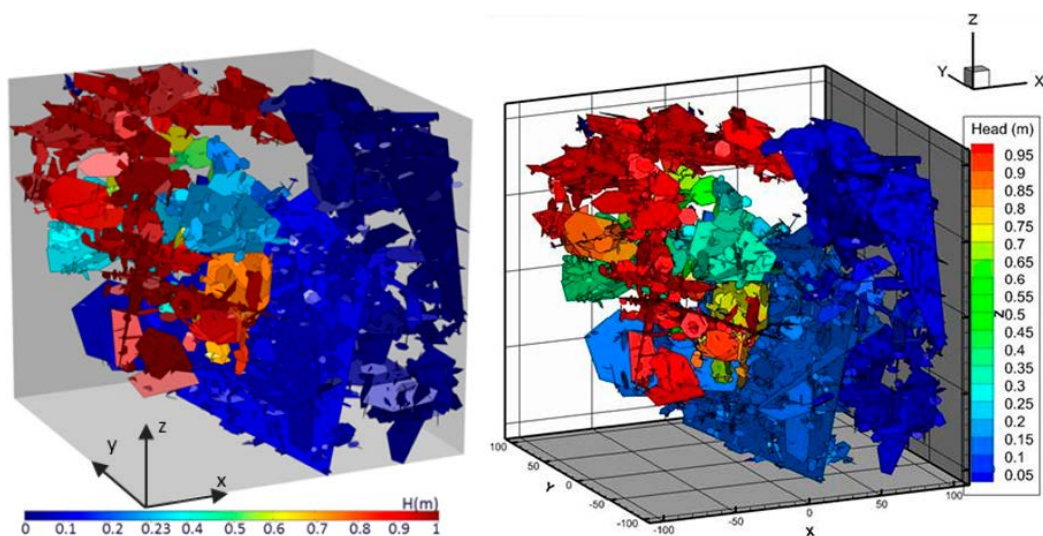


**Figure 4-3.** 3D hydraulic head distribution obtained from COMSOL (left) and MAFIC (right).

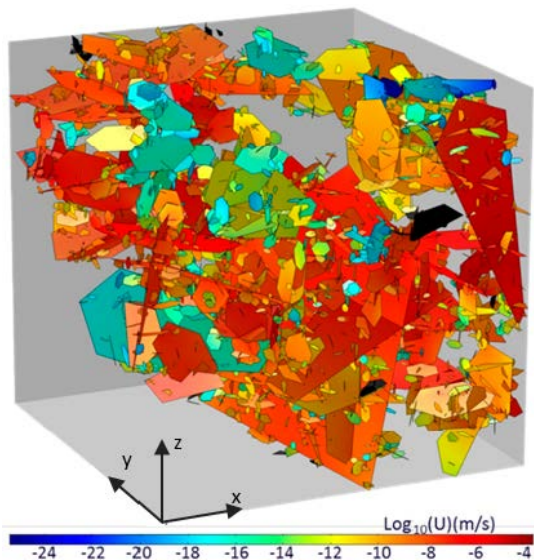


**Figure 4-4.** Darcy velocity magnitude in logarithmic scale. The black colour represents disconnected fractures with zero flow velocity.

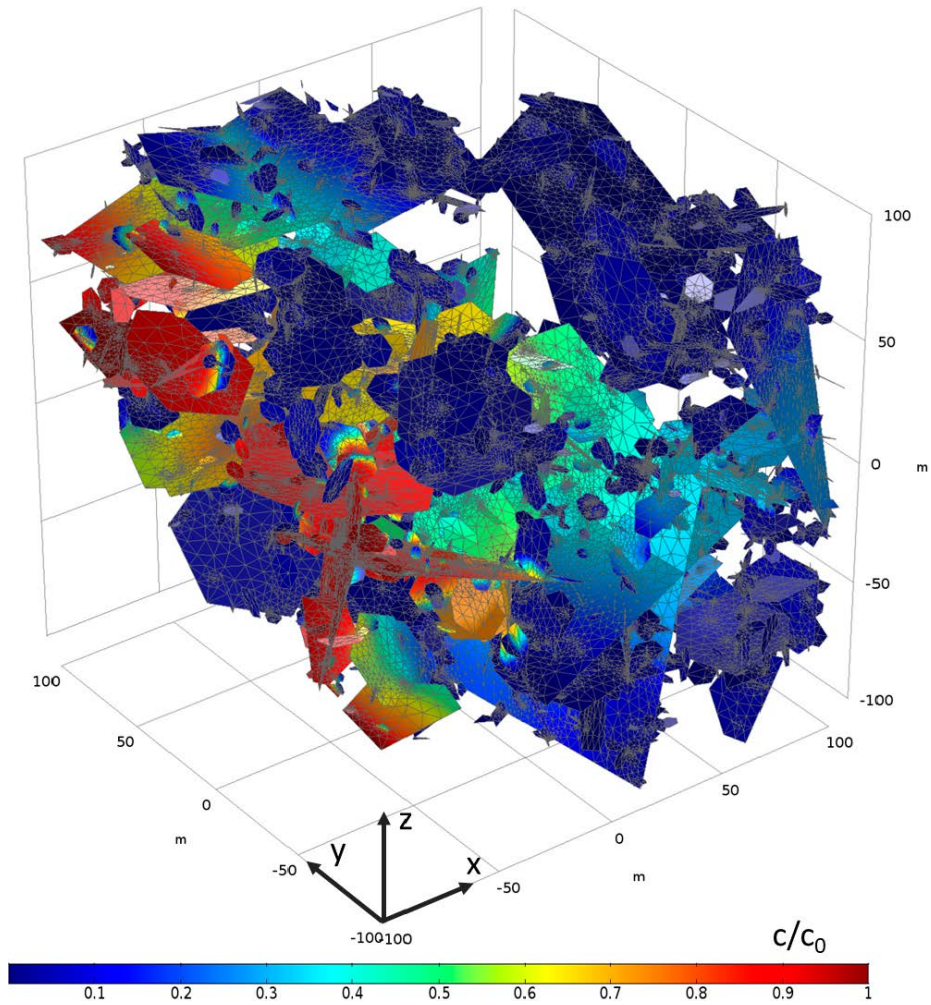
**Table 4-2. Groundwater mass balance (inflow and outflow) for the case evaluated.**

Inflow (kg/s)	Outflow (kg/s)	Number of mesh elements	Number of nodes	CPU time (s)
$3.4022 \times 10^{-6}$	$3.4805 \times 10^{-6}$	240721	130979	180

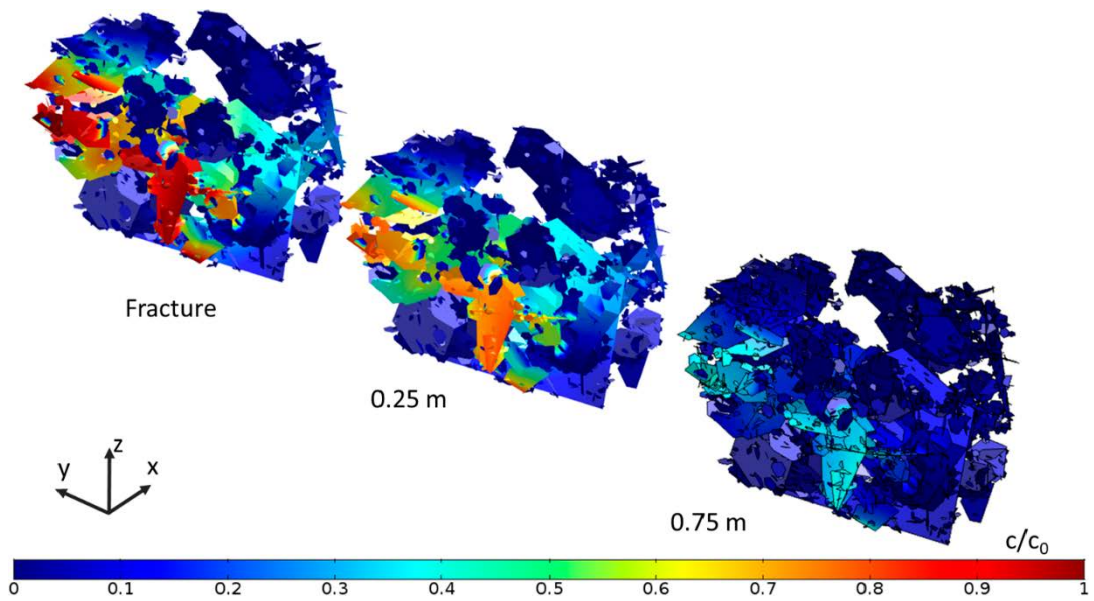
In order to validate the flow balance obtained, the same system has been simulated using MAFIC (Miller et al. 2001), a code to solve groundwater flow models generated in FracMan (Ford et al. 2008). The results obtained using MAFIC show inflow values of  $4.349 \times 10^{-6}$  kg/s, same order of magnitude as the inflow obtained from COMSOL (Table 4-2). The small discrepancy between the results might be caused by differences in the mesh resolution and also in the method to calculate the inflow and outflow values.

Figure 4-5 and Figure 4-6 show the concentration of chloride in the fracture-matrix system. Numerical results show also the presence of two preferential paths for solute transport. Thus, at the end of the simulation the chloride-magnesium plume spreads mainly along the upper part of the system and at the bottom. Note that the concentration distribution into the matrix represented by the 1D elements is not uniform, see Figure 4-6. This is because although the matrix is represented with one finite 1D element discretized with only two nodes, one node connecting the matrix and the fractures and another one located at a distance of 1 m from the matrix-fractures connection, and the properties of the 1D elements are considered homogenous, in this problem the concentration at the node which connects the matrix and the fractures is always higher than the one at the node located to 1 m from the matrix-fractures connection. Thus, after 200 years of simulation, the chloride concentration for most of the fractures at 0.75 m into the matrix is lower than half of the concentration entering through the boundary, and only few fractures present higher concentrations at this distance (see Figure 4-6). This indicates a strong retardation of the chloride plume migration induced by matrix diffusion processes.

Reactive transport results show the progressive replacement of calcite by dolomite due to the movement of the enriched chloride-magnesium plume (Figure 4-7). Although the incoming water is initially undersaturated with respect to dolomite, the mixing between the boundary water and the initial water in the matrix leads to oversaturation at the front of the magnesium-rich plume which causes dolomite to precipitate. Note that dolomite precipitation occurs mainly near the contact between matrix and fractures, and only a small amount of dolomite precipitates along the fractures (Figure 4-7). Numerical results also demonstrate that, in some areas, once calcite is depleted, mixing induces the dissolution of dolomite.



**Figure 4-5.** Normalized chloride distribution in the fractures at the end of the simulation. Grey lines show the finite element mesh.



**Figure 4-6.** Normalized chloride distribution at the end of the simulation in the fractures (left), 0.25 m (centre), and 0.75 m (right) into the matrix.

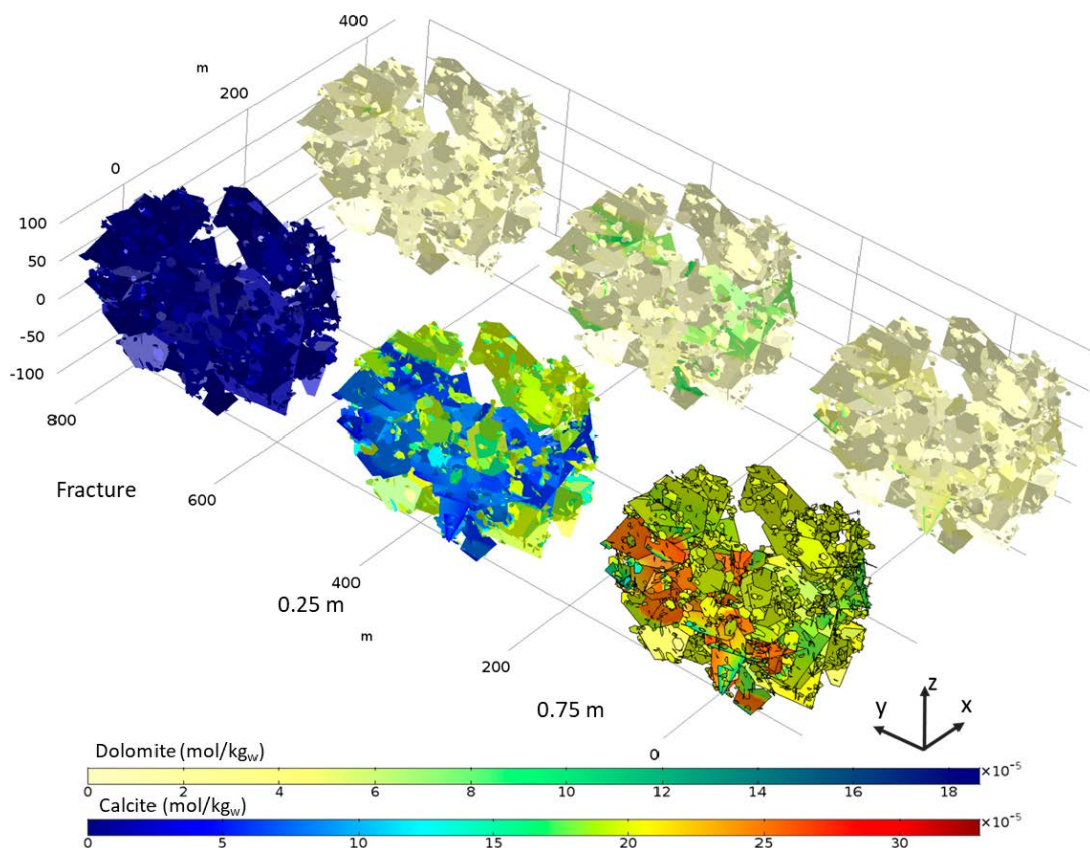


**Figure 4-7.** Concentration of calcite (bottom row) and dolomite (upper row) at the end of the simulation in the fractures (left), 0.25 m (centre), and 0.75 m (right) into the matrix.

#### 4.4 Performance quantification

This model has been used to evaluate the performance of the 1D matrix approach of iCP.

There are three different types of calculation steps taken during an iCP run: (i) the iCP time step which controls the information exchange between COMSOL and IPHREEQC and depends on the chemical system; (ii) the time step to store results; and (iii) the time step to save computed results. The results can be stored in memory or saved as a COMSOL output file.

iCP generates a .log file automatically that contains information of the duration of each process in iCP. In general, for each time-step during the calculation process the following three computation steps are taken:

1. The transport step that involves all the processes computed in COMSOL. One of these processes is the conservative transport simulation that translates the mass of the dissolved species coming from IPHREEQC. At the end of this step iCP exchanges the transported concentration to IPHREEQC.
2. The reactive step where IPHREEQC performs the geochemical calculation. After the geochemical calculations the concentration of the totals as well as the selected results (mineral concentration, sorbed mass, etc) are sent to COMSOL.
3. The saving step, when iCP stores the chemical results in memory or saves them in a COMSOL file depending on the saving settings selected by the user.

Table 4-3 summarizes the average, maximum and minimum duration of each computation step. The simulations were run on a computer with a i7-8700 processor with a CPU speed of 3.7 GHz, 6 cores and 64 GB of RAM memory. In this problem, the transport step is most time consuming. Thus, the total computational time is around 12.11 days and the transport step takes up approximately 95 % (11.15 days) of the total time. The transport step encompasses the total number of equations that COMSOL solves. In this example, the chemical system involves the transport of 7 species. Therefore,

the reactive transport model requires solving 7 systems of PDEs in 392 937 nodes for each transport step in COMSOL. The complexity of the finite element mesh and the fact that COMSOL is not parallelized make the transport step the most time consuming of the three stages. On the other hand, the chemical part requires solving 392 937 IPHREEQC batch calculations, one per node of the finite element mesh, which include both the fracture and matrix nodes. However, this part is well parallelized and iCP uses all the CPUs available to compute these reactions (Nardi et al. 2014). The saving time is long when dealing with large models. Thus, in the current example, iCP sometimes spends more time saving the results than solving the reactive step.

**Table 4-3. Summary of the computation time statistics for the iCP simulation.**

	Transport step	Reactive step	Saving time	Total time
Average time (s)	1 927.4	144.1	20.0	2 092.1
Maximum time(s)	4 050.0	192.0	460.0	4 470.0
Minimum time(s)	365.0	94.0	1.2	519.0
Total time (days)	11.15	0.83	0.12	12.11
Average contribution to the total duration of a time step	90.9 %	8.2 %	0.9 %	-

The analysis of the time step duration can be used to evaluate the performance of the code. Thus, the iCP efficiency can be analysed from the evolution of the time consumed in each step during the whole simulation. Figure 4-8 shows the duration of the time steps in iCP. Note that each time step has a different duration which ranges from 519 to 4470 s. Note also that there is no relationship between the duration of the time step and the steps where iCP stores the results.

Figure 4-9 shows the duration of all the steps of the simulation. The simulation had to be restarted twice during the execution of the simulation because of external problems not related to the simulation. The restart option allows to start the simulation from the last checkpoint saved. The figure shows that the duration of the steps is smaller after saving iCP results to file (yellow bars in Figure 4-9). The restart of the simulation is followed by some time steps with a small duration compared to the average time step duration. Steps 151 and 374 show that time step duration is significantly smaller after restart than before. There is also a clear increase of the time step duration with time that can be related to the generation of temporal files that are stored in memory until the simulation finishes or is stopped. However, this increase in the time step is not relevant for the overall simulation time in the analysed case.

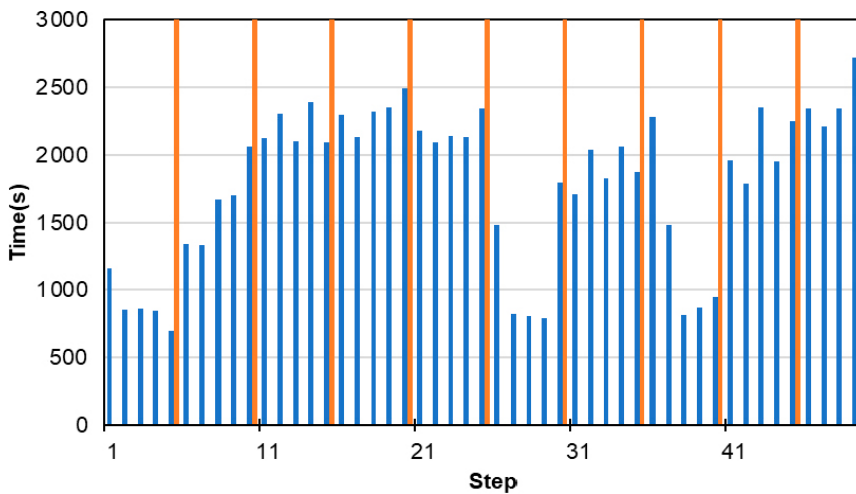


**Figure 4-8.** Zoom showing the duration of the first 50 computation steps (blue bars) of iCP for the application test as the sum of transport, reactive and saving times. The orange bars mark the steps where iCP saves the output file in the memory.

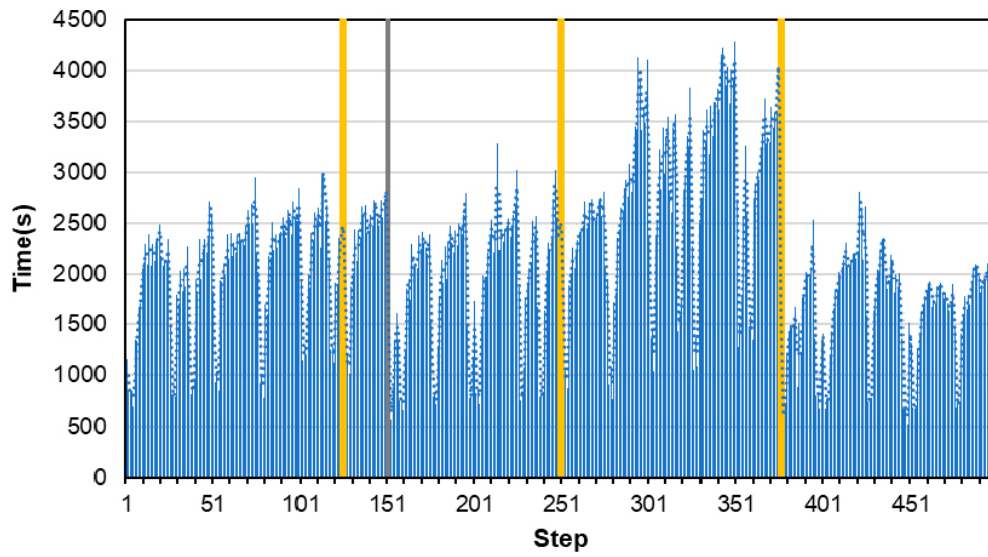


**Figure 4-9.** Blue bars showing the duration of each computation step of iCP for the application test as the sum of transport, reactive and saving times. The yellow bars mark the steps where iCP saves output files in the computer. The black bars show when the simulation was restarted.

## 5 Conclusions

A new version of iCP (interface COMSOL-PHREEQC) is presented. This version allows to solve reactive transport in discrete fractures with 1D matrix. The matrix is represented with a set of independent 1D elements connected to the fracture nodes (i.e., as an extra dimension). Thus, reactivity related to diffusion processes in the rock matrix can be simulated without a full three-dimensional representation of the matrix domain. This approach can be applied only when diffusion is the main mechanism for transport in the matrix.

The main advantages of this approach are that the matrix does not need to be fully represented in three dimensions, facilitating the generation of the geometry and mesh, and reducing the computational effort required to simulate the three-dimensional matrix and that the fractures are explicitly resolved as discrete structures and, therefore, the upscaling of transport and geochemical properties to build an equivalent continuous porous medium is not required.

The validation of the tool was carried out using existing examples of a single discrete fracture crossing a low permeability matrix.

The conservative transport was successfully validated by comparing the numerical results of iCP with an analytical solution (Tang et al. 1981) and the results of other codes. The 1D matrix approach can reproduce properly the effect of matrix diffusion.

There are no well-defined benchmark problems to validate the reactive transport in the 1D matrix, mostly due to the lack of numerical tools able to solve this type of problem. Therefore, problems involving geochemistry with fracture and matrix domains from the literature were used. These problems had been previously solved using either a continuous porous media (CPM) or a hybrid approach. Here, the discrete fracture is represented with 1D elements and a constant aperture that is specified as a parameter in the transport equation (Equation (2-2)). The matrix is simulated using the 1D matrix approach in iCP. This approach is compared with other representations of the fracture-matrix system:

- CPM in both the fracture and the matrix. These models were performed with iCP and Pflotran.
- Hybrid models with a 1D fracture and a 2D representation of the matrix. These models were performed with iCP as well.

The results for different approaches and codes were compared.

For all the verification tests evaluated, results when representing the rock matrix as 1D matrix are almost identical to the ones obtained using different representations with iCP (CPM and hybrid models). This agreement demonstrates that the 1D matrix approach is as valid as the two other approaches implemented in iCP.

However, when comparing the results from the different codes, the comparison is not ideal. The results obtained with iCP agree in terms of the spatial distribution of pH and major ions with the results from Pflotran and the code used in Steefel and Lichtner (1998). Also, the scaling between the chemical composition of the fracture and the matrix with the Peclet number, as presented by Steefel and Lichtner (1998), is reproduced. However, different precipitation rates (mass of mineral precipitated/time) are obtained. The reason is that thermodynamic databases and the definition of the kinetic model are not fully consistent between the two codes. The development of a consistent thermodynamic database for both applications would be required to perform a fair comparison. The discrepancies are intrinsic to the different way of treating the mineral reactions in the different codes, and not to the representation of the matrix in the 1D matrix approach.

The difficulties in the validation highlight the need of well-defined reactive transport problems involving fractures and matrix and the criticality of having consistent thermodynamic databases to perform code comparisons.

The applicability of this tool to solve reactive transport in complex geometries involving discrete fracture networks is illustrated with a 3D application of dolomitization in a fractured carbonate-rich rock. In this case, the DFN consists of 3 531 hexagonal fractures. Due to the lack of other codes able to solve this type of problem, this case could be replicated with a reactive model with an ECPM approximation. However, the results would not be comparable due to the underlying assumptions in the upscaling of the transport and geochemical properties needed to perform the ECPM. The CPU time required to run this 200-year long dolomitization simulation with iCP is 12 days, which is reasonable considering the complex geometry of the problem considered.

This is, together with the recently available version of ConnectFlow, the only tools available to solve reactive transport in DFNs with diffusion and reactions in the matrix. This approximation is still far from being usable to model reactive transport for a whole repository site given the large temporal and spatial scale required. However, it is suitable to be used in smaller scale applications for the near-field such as the simulation of degradation of fractured concrete or the simulation of the role of the Excavation Damaged Zone (EDZ) in the release of radionuclides and concrete leaching water from the repository vaults to the geosphere.

## References

SKB's (Svensk Kärnbränslehantering AB) publications can be found at [www.skb.com/publications](http://www.skb.com/publications).

**Bear J, 1972.** Dynamics of fluids in porous media. New York: Elsevier.

**Charlton S R, Parkhurst D L, 2011.** Modules based on the geochemical model PHREEQC for use in scripting and programming languages. *Computers & Geosciences* 37, 1653–1663. <https://doi.org/10.1016/j.cageo.2011.02.005>

**COMSOL, 2017.** COMSOL Multiphysics. Reference manual, version 5.3. Burlington, MA: COMSOL Inc.

**Darcy H, 1856.** Les fontaines publiques de la ville de Dijon. Exposition et application des principes à suivre et des formules à employer dans les questions de distribution d'eau: ouvrage terminé par un appendice relatif aux fournitures d'eau de plusieurs villes au filtrage des eaux et à la fabrication des tuyaux de fonte, de plomb, de toile et de bitume. Paris: Dalmont. (In French.)

**Ford N T, Silverton T R, Cottrell M G, 2008.** Rock mass characterisation of a prospective base metal deposit using a combined FracMan/ELFEN approach. In Potvin Y, Carter J, Dyskin A, Jeffrey R (eds). SHIRMS 2008: Proceedings of the First Southern Hemisphere International Rock Mechanics Symposium, Perth. Australian Centre for Geomechanics, 605–617.

**Idiart A, Laviña M, Coene E, 2019.** Modelling of concrete degradation – Hydro-chemo-mechanical processes. Report for the safety evaluation SE-SFL. SKB R-19-12, Svensk Kärnbränslehantering AB.

**Idiart A, Laviña M, Grandia F, Pont A, 2020.** Reactive transport modelling of montmorillonite dissolution. Report for the safety evaluation SE-SFL. SKB R-19-15, Svensk Kärnbränslehantering AB.

**Iraola A, Trinchero P, Karra S, Molinero J, 2019.** Assessing dual continuum method for multi-component reactive transport. *Computers & Geosciences* 130, 11–19. <https://doi.org/10.1016/j.cageo.2019.05.007>

**Jacobs, 2021.** ConnectFlow, Technical summary, Version 12.3. Didcot, UK: Jacobs. Available at: [https://www.connectflow.com/resources/docs/conflow\\_technical.pdf](https://www.connectflow.com/resources/docs/conflow_technical.pdf)

**Jacques D, 2009.** Benchmarking of the cement model and detrimental chemical reactions including temperature dependent parameters. Project near surface disposal of category A waste at Dessel. NIROND-TR 2008–30 E, ONDRAF/NIRAS, Belgium.

**Lichtner P C, Hammond G E, Lu C, Karra S, Bisht G, Andre B, Mills R T, Kumar J, 2015.** PFLOTRAN user manual: A massively parallel reactive flow and transport model for describing surface and subsurface processes. LA-UR-15-20403, Los Alamos National Laboratory. <https://www.osti.gov/biblio/1168703-pflotran-user-manual-massively-parallel-reactive-flow-transport-model-describing-surface-subsurface-processes>

**Miller I, Lee G, Dershowitz W, 2001.** MAFIC, Matrix / fracture interaction code with head and solute transport, User documentation, version 2.0.

**Nardi A, Idiart A, Trinchero P, de Vries L M, Molinero J, 2014.** Interface COMSOL–PHREEQC (iCP), an efficient numerical framework for the solution of coupled multiphysics and geochemistry. *Computers & Geosciences* 69, 10–21. <http://dx.doi.org/10.1016/j.cageo.2014.04.011>

**Parkhurst D L, Appelo C, 2013.** Description of input and examples for PHREEQC version 3: a computer program for speciation, batch-reaction, one-dimensional transport, and inverse geochemical calculations. U.S. Geological Survey. <https://pubs.usgs.gov/tm/06/a43/>

**Parkhurst D L, Kipp K L, Engesgaard P, Charlton S R, 2004.** PHAST – A program for simulating ground-water flow, solute transport, and multicomponent geochemical reactions. U.S. Department of the Interior, U.S. Geological Survey. <https://pubs.usgs.gov/tm/2005/tm6A8/>

**Sampietro D, Abarca E, Molinero J, 2022a.** iCP version 2.0: A numerical tool for solving reactive transport in fractured media. SKB R-21-09, Svensk Kärnbränslehantering AB.

**Sampietro D, Abarca E, Sáinz-García A, Molinero J, 2022b.** A combined hydrogeology and radionuclide transport model of the SFL near-field. SKB R-21-12, Svensk Kärnbränslehantering AB.

- Steefel C I, Lichtner P C, 1994.** Diffusion and reaction in rock matrix bordering a hyperalkaline fluid-filled fracture. *Geochimica et Cosmochimica Acta* 58, 3595–3612. [https://doi.org/10.1016/0016-7037\(94\)90152-X](https://doi.org/10.1016/0016-7037(94)90152-X)
- Steefel C I, Lichtner P C, 1998.** Multicomponent reactive transport in discrete fractures: I. Controls on reaction front geometry. *Journal of Hydrology* 209, 186–199. [https://doi.org/10.1016/S0022-1694\(98\)00146-2](https://doi.org/10.1016/S0022-1694(98)00146-2)
- Steefel C I, Yabusaki S B, 1996.** OS3D/GIMRT software for modeling multicomponent-multidimensional reactive transport. Report. Pacific Northwest National Laboratory, Richland, Washington. <https://www.osti.gov/biblio/754946-os3d-gimrt-software-modeling-multicomponent-multidimensional-reactive-transport>
- Sudicky E A, Frind E O, 1982.** Contaminant transport in fractured porous media: Analytical solutions for a system of parallel fractures. *Water Resources Research* 18, 1634–1642. <https://doi.org/10.1029/WR018i006p01634>
- Svensson U, Ferry M, Kuylenstierna H-O, 2010.** DarcyTools version 3.4 – Concepts, methods and equations. SKB R-07-38, Svensk Kärnbränslehantering AB.
- Tang D H, Frind E O, Sudicky E A, 1981.** Contaminant transport in fractured porous media: Analytical solution for a single fracture. *Water Resources Research* 17, 555–564. <https://doi.org/10.1029/WR018i006p01634>

SKB is responsible for managing spent nuclear fuel and radioactive waste produced by the Swedish nuclear power plants such that man and the environment are protected in the near and distant future.

**skb.se**